NASA CONTRACTOR REPORT

NASA CR-1513

THE DETERMINATION OF ATMOSPHERIC TEMPERATURE PROFILES FROM PLANETARY LIMB RADIANCE PROFILES

by James W. Burn and William G. Uplinger

Prepared by
LOCKHEED MISSILES & SPACE COMPANY
Sunnyvale, Calif.
for Langley Research Center

NATIONAL AERONAUTICS AND SPACE ADMINISTRATION • WASHINGTON, D. C. • FEBRUARY 1970

THE DETERMINATION OF ATMOSPHERIC TEMPERATURE PROFILES FROM PLANETARY LIMB RADIANCE PROFILES

By James W. Burn and William G. Uplinger

Prepared under Contract No. NAS 1-8048 by
LOCKHEED MISSILES & SPACE COMPANY
Sunnyvale, Calif.

for Langley Research Center

NATIONAL AERONAUTICS AND SPACE ADMINISTRATION

For sale by the Clearinghouse for Federal Scientific and Technical Information
Springfield, Virginia 22151 – Price $3.00

ABSTRACT

A study was conducted to demonstrate the feasibility of inverting planetary limb radiance to infer atmospheric temperature structure. The method is based on the existence of a closed form solution to the equation of radiative transfer for a non-isothermal atmosphere specifically linear temperature gradients. Feasibility has been demonstrated by deriving a convergence theorem and stability criteria and by numerically inverting limb radiance data for various climatological models and Project Scanner experimental data. Inversion results over the altitude range of 30 to 60 km were generally accurate to less than $\pm 2°K$ in the stratosphere with peak errors of approximately $\pm 3°K$. Inversion results for the mesophere indicate that accuracies comparable or better than MRN data are possible.

Two methods have previously been developed for determining atmospheric temperature of the earth from an orbiting satellite:

- Spectral Probing to Different Atmospheric Altitudes. This method involves time-consuming inversion of a matrix and has stability problems in the presence of noise.
- Inversion by Iterative Integration of the Equation of Radiative Transfer. This is a straightforward method, but may require more sophisticated computing facilities than the direct method proposed in this report.

This study presents an alternative method that promises to be rapid and efficient. Atmospheric temperature is inferred from a normalized limb radiance profile based on a closed-form solution of the equation of radiative transfer. This ratio approach tends to minimize noise in the solution of the nonlinear inversion equation.

Basic assumptions applicable to this study are set forth, and the equation of radiative transfer is solved for isothermal atmospheres. Specifically, a solution is obtained for three transmissivity models: a Beer's Law model, an error-function model, and the Goody model. Calculation with a Beer's Law transmissivity model provides a good approximation of a limb radiance profile when the limb radiance at a single frequency is calculated from the error-function transmissivity model and then integrated over the 14−16 CO_2 band. Use of Beer's Law permits the development of a relatively simple inversion equation. The limb radiance is then rewritten in a form that is linear in thermal equivalent altitude (geometric altitude normalized by scale height).

The linearized limb radiance equation can be written as a nonlinear equation in temperature and solved iteratively. It is demonstrated that this solution for temperature converges rapidly, and the solution is stable for isothermal atmospheres. Numerical results, which are obtained for a 200°K isothermal atmosphere, demonstrate the basic inversion technique.

The equation of radiative transfer is solved for an atmosphere with a linear temperature gradient and with a Beer's Law transmissivity model. A linearized limb radiance equation, similar to that mentioned above, is derived.

The inversion equation is developed, and convergence is again demonstrated although the solution is conditionally stable for this more general case. Both the absolute and relative errors are shown to decrease rapidly on successive iterations. A check is made on the relative error on each iteration to prevent the solution from diverging.

Tentative feasibility of this inversion technique is demonstrated by results from computer runs. A 200°K isothermal atmosphere agrees with the predictions made by the convergence theorem. A mean January, 50°N atmosphere is seen to converge in a similar manner and is found to behave properly in the presence of a bias and noise.

Finally, mean absorption coefficients are computed from experimental Project Scanner data and MRN data. These mean absorption coefficients are used to invert four limb scans. The results demonstrate the stability of the inversion technique in the presence of noise and yield inferred temperatures which appear to be within the accuracy of MRN data.

Further study is required to answer many questions which arose during the course of this effort and to improve on simplifying approximations that later proved to be inadequate. Specifically, the limitations of certain starting assumptions need to be fully explored and the nature of the mean absorption coefficient needs to be investigated. Also, the method of assuring stability of the solution must be further developed. Finally, the inversion technique must be tried on a large number of climatological model atmospheres that are representative of latitudinal and seasonal variations to assure the general applicability required for operational use. None of these studies will prove to be fundamentally difficult as tentative feasibility is demonstrated both theoretically and numerically in this report.

FOREWORD

This report by Lockheed Missiles & Space Company (LMSC) presents the results of a study of the feasibility of inferring upper atmospheric temperature structure by inverting planetary limb radiance profiles. This is a first study based on ideas which originated at LMSC. The effort reported here was performed for Langley Research Center, National Aeronautics and Space Administration, under Contract No. NAS1-8048.

The authors wish to acknowledge the support, encouragement, and helpful suggestions in preparation of this report of Messrs. John Dodgen and Howard Kurfman and the two Technical Monitors Lloyd Keafer, Jr. and Richard E. Davis, all of Langley Research Center. We also appreciate the many helpful technical discussions with Mrs. Ruth I. Whitman and Mr. Thomas B. McKee, both of Langley Research Center, and with Dr. Fredrick E. Alzofon of Lockheed Missiles & Space Company.

CONTENTS

ILLUSTRATIONS

TABLES

SYMBOLS

B	blackbody radiance, watts/centimeter^2/steradian
B'	radiance change due to atmospheric temperature gradient
C'	radiance change due to temperature variation from T^o, the equivalent peak blackbody temperature
C_2	second Planck radiation coefficient, 1.4380 cm °K
d	line separation, meters
G	planetary thermal constant
G_o	gravitational constant, meters/second^2
g	acceleration due to gravity, 980 centimeters/second^2
H	scale height, meters
$K_{n/2}(\gamma)$	K function with positive argument
$K_{n/2}(-\gamma)$	K function with negative argument
k_{abs}	absorption coefficient, centimeters^2/gram
k	Boltzmann's constant, 1.3804×10^{-6} erg/°K
L	temperature gradient, °K/meter
ℓ	position measured from horizon, meters
M_e	mass of earth, grams
m	mass of molecule, grams (28.964)
N	radiance, watt/centimeters^2/steradian
P	pressure, millibars
R_e	radius of earth, kilometers
S	line strength, centimeters^2/gram/second
s	path length, meters

T	temperature, °K
T^o	equivalent blackbody temperature for the radiance at z20
u	mass per unit area, grams/centimeter^2
W (z')	total weighting function at altitude z' for a radially symmetric atmosphere
w	mixing ratio
x	thermal equivalent altitude
x'	$Su/2\pi$
z	altitude, meters
z' , z''	dummy variables of integration with altitude, meters
α	half-width, meters
β	$2\pi\ \alpha/d$
Γ	relative error in γ
γ	scale height gradient
$\overline{\gamma}$	mean scale height gradient above the horizon altitude
Δ	relative temperature error, °K
δ	absolute temperature error, °K
ϵ	absolute error in x
η	inflection altitude
η_e	altitude related to the inflection altitude for error function transmissivity model
λ	wavelength, microns
ν	frequency, cm^{-1}
ρ	density, grams/meter^3
τ	transmission
τ_o	optical thickness of the atmosphere

SECTION 1. – ISOTHERMAL ATMOSPHERES

1.1 Introduction

This report is concerned with the specific problem of inverting limb radiance data to infer atmospheric temperature structure. The method described in this report is necessarily restricted to wave lengths corresponding to absorption bands of the principal absorbers and emitters in the atmosphere; therefore, temperature structure can be inferred only from the lower stratosphere through the mesophere, approximately 20 km to 60 km. For simplicity in demonstrating the feasibility of inversion by the particular method described, only the 15 μCO_2 band will be considered.

Carbon dioxide is assumed to be uniformly mixed by volume throughout the atmosphere, at least up to 90 km or 100 km, where theoretical studies (ref. 1) indicate that dissociation of CO_2 molecules by ultraviolet radiation becomes dominant. This is a reasonable assumption since neither sinks nor sources of CO_2 exist within the atmosphere, and the CO_2 introduced into the atmosphere should become uniformly mixed by convection.

A single absorbing line is assumed to have a Lorentz or collision-broadened line shape. It is recognized that a mixed Doppler-Lorentz line shape increases the absorption above the amount predicted by band models that assume a Lorentz shape. Although the Doppler half-width and Lorentz half-width are equal at approximately 31-km altitude, this is not the altitude at which the Doppler shape becomes important. Rodgers and Walshaw (ref. 2) conclude that for a vertical atmospheric path the Doppler line shape should be considered above 52 km. However, a horizon profile involves longer atmosphere paths since the path is horizontal with a consequently greater width of total absorption. The altitude at which the Doppler line shape becomes important is, therefore, above 52 km.

The atmosphere is assumed to be in local thermodynamic equilibrium. If molecular collisions are frequent enough so that the supply of excited state meets the demand, the Planck blackbody law is valid. If collisions are less frequent, there are not enough molecules available for emission, and the radiation is less than Planck radiation. Departures from the Planck function become important only when the time necessary to reestablish equilibrium, the relaxation time defined as the ratio of the number of collisions required to restore the energy levels to the average number of collisions per second, corresponding to the atmospheric density, is the same order of magnitude as the radiative lifetime for spontaneous emission. Since the number of collisions per second is directly proportional to pressure and inversely proportional to the square root of temperature (ref. 3), the relaxation time of 2×10^{-6} sec at 220° K and 1 atmosphere (ref. 4) increases rapidly with altitude becoming equal to the radiative lifetime of 0.37 sec (ref. 4) at a pressure of 5.4×10^{-3} millibars. For the 1962 Standard Atmosphere, this occurs at an altitude of 85 km.

Thus, it seems that the primary assumptions required for the remaining discussion are reasonable for inferring temperature structure below 75 or 80 km with the possible exception of the line shape. This effect will be small and will require, at the most, a minor correction.

With the assumption of local thermodynamic equilibrium, the spectral radiance seen from a path that does not intersect the earth's surface (fig. 1) can be derived from the one-dimensional equation of radiative transfer and is given by:

$$N_\nu = - \int_0^\infty B_\nu \frac{\partial \tau_\nu}{\partial s} ds \tag{1}$$

where

N_ν = spectral radiance

B_ν = Planck blackbody spectral radiance

τ_ν = transmission of the atmosphere at frequency ν

s = path length through the atmosphere

The partial differential of transmission with respect to path $\partial\tau/\partial s$ is called the weighting function as it determines the contribution to the total radiance of the blackbody radiation for the temperature of each increment of path. Therefore, it is important that we know how the weighting function varies along the path.

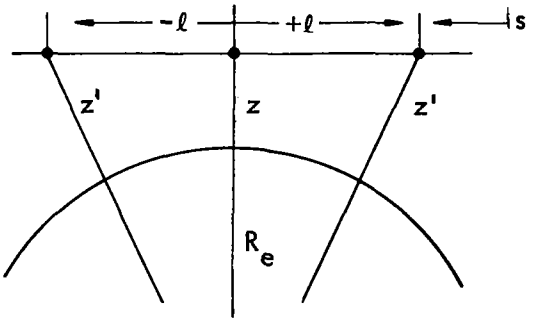

Fig. 1 Horizon Geometry

Transmission at frequency ν is given by the exponential function whose argument is the product of an absorption coefficient and the optical path.

$$\tau_\nu = \exp (- k_{abs\nu} u) \tag{2}$$

where

$k_{abs\nu}$ = absorption coefficient at frequency ν

u = optical path, gm/m^2

$$u = \int_{s=0}^\infty w \rho ds \tag{3}$$

where

w = mixing ratio

ρ = density of the absorbing medium

It will be found more useful to rewrite Eq. (2) as follows:

$$\tau_\nu = \exp\left[-\tau_{o\nu}\left(\frac{1}{w\rho_o}\frac{u}{H}\right)\right] \tag{4}$$

and $\tau_{o\nu}$ is the optical thickness of the atmosphere at wavelength ν given by

$$\tau_{o\nu} = wk_\nu \rho_o H \tag{5}$$

H is defined as:

$$H = \frac{kT}{mg} \tag{6}$$

where

k = Boltzmann's constant (1.3804×10^{-6} erg/°K)

T = temperature

m = molecular weight of a molecule (28.964)

g = acceleration of gravity (980 centimeters/sec^2)

The term $(u/w\rho_o H)$ is the mass of absorber per unit of area in a length H reduced to standard conditions and is called the reduced absorber mass.

From Eqs. (2) and (3), the weighting function is found to be given by:

$$\frac{\partial\tau}{\partial s} = -k_{abs\nu}\,\tau_\nu \frac{\partial u_s}{\partial s} \tag{7a}$$

$$= -\tau_{o\nu}\,\tau_\nu \frac{\partial\left(\frac{1}{w\rho_o}\frac{u}{H}\right)}{\partial s} \tag{7b}$$

$$= -k_{abs\nu}\,\tau_v\, w\rho \tag{7c}$$

Thus, the weighting function is a direct function of the number of absorbing molecules and is related to the strength of the absorbing molecule directly by the k_ν term and indirectly through the transmission. Since the density is greatest at the point of

closest approach to the surface (altitude z in fig. 1) and the transmission is continuously decreasing, the weighting function would be expected to peak in front of the point of closest approach.

This section deals with isothermal atmospheres, and Eq. (1) can be rewritten as follows:

$$N_\nu = -B_\nu \int_{s=0}^{s=\infty} \frac{\partial \tau_\nu}{\partial s} ds \tag{8}$$

With the appropriate change of the limits of integration this becomes,

$$N_\nu = -B_\nu \int_{1}^{\tau(s=\infty)} d\tau_\nu \tag{9}$$

which can be integrated directly to yield

$$N_\nu = B_\nu \left[1 - \tau_\nu(s = \infty)\right] \tag{10}$$

The radiance in a given bandwidth, therefore, is found by integrating Eq. (10) over frequency. If the bandwidth is small, N_ν and B_ν can be considered constants over the bandwidth. The integration is then only over the factor $(1 - \tau)$, and the appropriate band models can be used. Equation (10) is modified for a narrow bandwidth by replacing ν by $\Delta\nu$ and using the appropriate $(1 - \tau)$ for the band model considered. In the remaining discussion, $\Delta\nu$ has been omitted but is implied. The modified equation is the basic equation that is solved to determine the theoretical limb radiance profile.

1.2 Beer's Law Transmission

For uniformly mixed gray atmospheres as considered by King (ref. 5) and the weak-line approximation to many transmission functions, the transmission is given by Eq. (2) where the absorption coefficient is a constant throughout the atmosphere. From the perfect gas law and the hydrostatic equation, the density as a function of altitude z is given by:

$$\rho = \rho_o \exp(-z/H) \tag{11}$$

Since density is a function of altitude z, path ℓ must also be expressed as a function of altitude z. By the Pythagorean theorem,

$$\ell^2 + (R_e + z)^2 = (R_e + z')^2 \tag{12}$$

and solving for ℓ

$$\ell = \left\{\left[2R_e + (z' + z)\right](z' - z)\right\}^{1/2} \tag{13}$$

Since $(z' + z) << 2R_e$

$$\ell = \left[2R_e(z' - z)\right]^{1/2} \tag{14}$$

Also, $ds = -d\ell$ and

$$ds = -\frac{R_e\, dz'}{\left[2R_e(z' - z)\right]^{1/2}} \tag{15}$$

The value of u_s, for ℓ positive at an altitude z' is given by:

$$u_s = -\int_{\infty}^{z'} \frac{w\rho_o R_e \exp(-z''/H)}{\left[2R_e(z'' - z)\right]^{1/2}}\, dz'' \tag{16}$$

or

$$u_s = \frac{(2R_e)^{1/2}}{2} w\rho_o \int_{z'}^{\infty} \frac{\exp(-z''/H)}{(z'' - z)^{1/2}}\, dz'' \tag{17}$$

This integral can be evaluated, yielding

$$u_s = \frac{H}{2}\left(\frac{2\pi R_e}{H}\right)^{1/2} w\rho_o \left\{1 - \operatorname{erf}\left(\frac{z' - z}{H}\right)^{1/2}\right\} \exp(-z/H) \tag{18}$$

similarly, for negative ℓ

$$u_s = \frac{H}{2}\left(\frac{2\pi R_e}{H}\right)^{1/2} w\rho_o \left\{1 + \operatorname{erf}\left(\frac{z' - z}{H}\right)^{1/2}\right\} \exp(-z/H) \tag{19}$$

Thus, the reduced absorber mass becomes (for $\pm \ell$)

$$\left(\frac{1}{w\rho_o}\frac{u}{H}\right)_s = \frac{1}{2}\left(\frac{2\pi R_e}{H}\right)^{1/2} \left\{1 \pm \text{erf}\left(\frac{z' - z}{H}\right)^{1/2}\right\} \exp(-z/H) \tag{20}$$

This expression states that the basic shape of the reduced absorber mass function in terms of the differential altitude $(z' - z)$ is independent of altitude and the magnitude decreases exponentially with altitude. From Appendix A, the planetary thermal constant G is defined by:

$$G = \frac{1}{2}\ell n\left(\frac{2\pi R_e}{H}\right) \tag{21}$$

and defining the thermal equivalent altitude x as

$$x = z/H \tag{22}$$

Equation (20) becomes (for $\pm \ell$)

$$\left(\frac{1}{w\rho_o}\frac{u}{H}\right)_s = \frac{1}{2}\left\{1 \pm \text{erf}\left(\frac{z' - z}{H}\right)^{1/2}\right\} \exp(G - x) \tag{23}$$

The reduced absorber mass for $G - x = 0$ is plotted in fig. 2 as a function of the thermal equivalent differential altitude $(z' - z)/H$. Equation (23) can be expressed in terms of ℓ

$$\left(\frac{1}{w\rho_o}\frac{u}{H}\right)_s = \frac{1}{2}\left\{1 - \text{erf}\left[\sqrt{\pi}\,\frac{\ell}{H}\exp(G)\right]\right\} \exp(G - x) \tag{24}$$

When $\ell = +\infty\,(s = 0)$, $u_s = 0$ and when $\ell = -\infty\,(s = \infty)$,

$$\left(\frac{1}{w\rho_o}\frac{u}{H}\right) = \exp(G - x) \tag{25}$$

as would be expected for a uniformly mixed isothermal atmosphere.

It is clear that most of the limb radiance arises from a layer less than 1 scale height thick, and the importance of higher layers vanishes rapidly. It is this important result that makes feasible a reasonably simple unique solution of the temperature structure from the inversion of limb radiance.

Substituting Eq. (23) into Eq. (4) yields the equation for transmission to any point along the path (for $\pm \ell$).

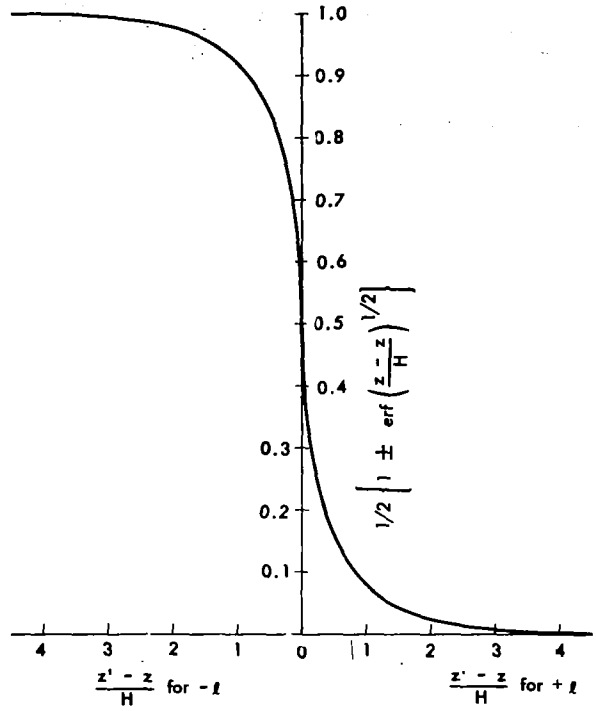

Fig. 2 Reduced Absorber Mass for a Thermal Equivalent Altitude Equal to G

$$\tau_s = \exp\left\{-\frac{\tau_o}{2}\left[1 \pm \text{erf}\left(\frac{z' - z}{H}\right)^{1/2}\right]\right\}\exp(G - x) \tag{26}$$

By some algebraic manipulation, Eq. (26) can be written as:

$$\tau_s = \left\{\exp - \frac{1}{2}\left[1 \pm \text{erf}\left(\frac{z' - z}{H}\right)^{1/2}\right]\right\}^{\exp(G - x + \ell n\, \tau_o)} \tag{27}$$

Thus, it is seen that the transmission is a basic transmission ($x = G + \ell n\, \tau_o$) raised to a power determined by the thermal equivalent altitude. Defining

$$\eta = H(G + \ell n\, \tau_o) \tag{28}$$

and recalling the definition of x, Eq. (28) can be written

$$\tau_s = \left\{ \exp - \frac{1}{2} \left[1 \pm \operatorname{erf} \left(\frac{z' - z}{H} \right)^{1/2} \right] \right\} \exp - \left(\frac{z - \eta}{H} \right) \tag{29}$$

This is plotted in fig. 3 for three values of $(z - \eta)/H$.

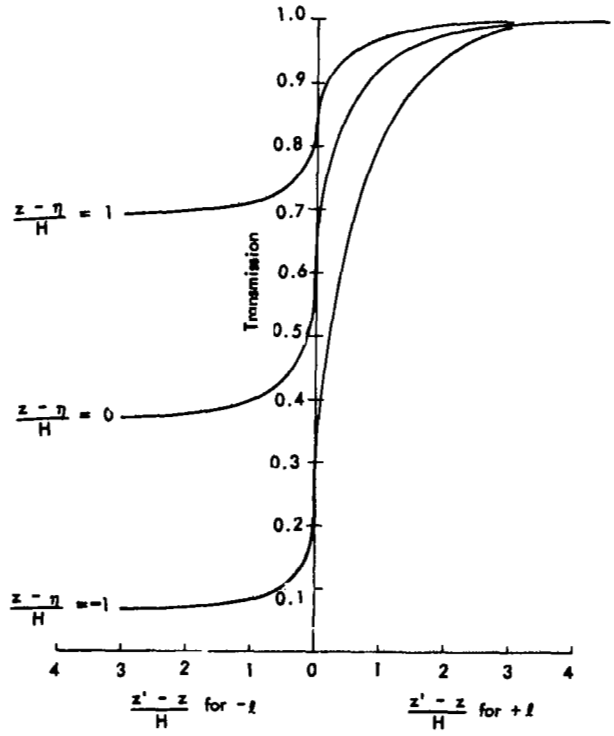

Fig. 3 Transmission Along a Horizon Path Corresponding to the Inflection Altitude and ± 1 Scale Height

When $s = \infty$, Eq. (29) becomes

$$\tau = \exp \left[-\exp - \left(\frac{z - \eta}{H} \right) \right] \tag{30}$$

From Eqs. (3), (7b), (11), and (27), the desired expression for the weighting function can be found (for $\pm \ell$)

$$\frac{\partial \tau}{\partial s} = -\tau_o \frac{w}{H} \exp(-z'/H) \left\{ \exp - \frac{\tau_o}{2} \left[1 \pm \operatorname{erf} \left(\frac{z' - z}{H} \right)^{1/2} \right] \right\} \exp(G - x) \tag{31}$$

which can be rewritten as (for $\pm \ell$)

$$\frac{\partial \tau}{\partial s} = -\frac{2}{H} \exp(-G) \left[\frac{\tau_o}{2} \exp(G - x)\right] \left\{\exp - \left[\frac{\tau_o}{2} \exp(G - x)\right]\right.$$

$$\left.\left[1 \pm \operatorname{erf} \left(\frac{z' - z}{H}\right)^{1/2}\right]\right\} \exp - \left(\frac{z' - z}{H}\right) \tag{32}$$

or as

$$\frac{\partial \tau}{\partial s} = -\frac{2}{H} \exp(-G)\, y \exp(-y) \exp\left[\pm y \operatorname{erf} \left(\frac{z' - z}{H}\right)^{1/2}\right] \exp - \left(\frac{z' - z}{H}\right) \tag{33}$$

where

$$y = \frac{\tau_o}{2} \exp(G - x) \tag{34}$$

or more conveniently by substituting Eqs. (22) and (28)

$$y = \frac{1}{2} \exp - \left(\frac{z - \eta}{H}\right) \tag{35}$$

The functional form of Eq. (33)

$$\exp\left[\pm y \operatorname{erf} \left(\frac{z' - z}{H}\right)^{1/2}\right] \exp - \left(\frac{z' - z}{H}\right)$$

is plotted in fig. 4 for $x = \eta$ and 1 scale height above and below inflection altitude η.

The curves in fig. 4 have two values of the ordinate for each value of $(z' - z)/H$, corresponding to plus and minus values of ℓ. The difference between the two curves is the different value of transmission, as seen in fig. 3. It is instructive to determine the contribution from each altitude, summing the contribution from plus and minus ℓ. Denote $W(z')$ as the contribution at altitude z'. Then

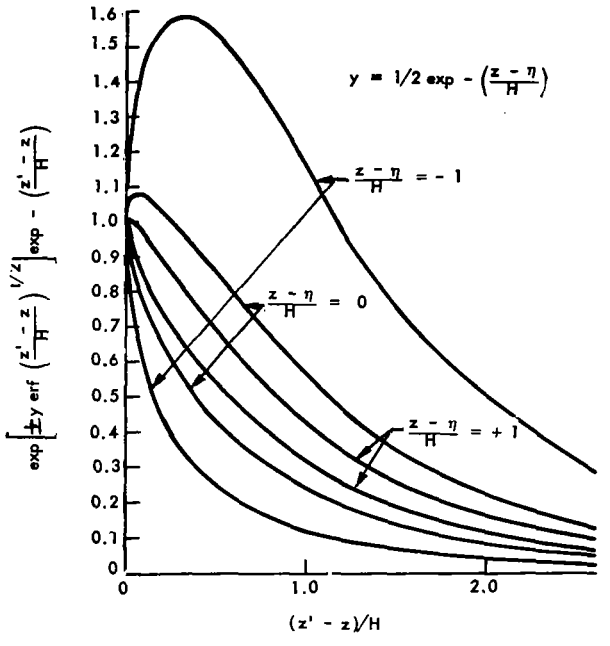

Fig. 4 Functional Form of the Weighting Function for an Altitude Equal to the Inflection Altitude and ±1 Scale Height

$$W(z') = \frac{-2}{H} \exp(-G)\, y \exp(-y) \exp\left[-\left(\frac{z' - z}{H}\right)\right] \left\{\exp\left[-y \operatorname{erf}\left(\frac{z' - z}{H}\right)^{1/2}\right] + \exp\left[y \operatorname{erf}\left(\frac{z' - z}{H}\right)^{1/2}\right]\right\} \quad (36)$$

Consider the case where $y \operatorname{erf} (z' - z/H)^{1/2}$ is much less than one. Only the first two terms in the series expansion of the exponential need be kept and $W(z')$ becomes

$$W(z') = \frac{-4}{H} \exp(-G)\, y \exp(-y) \exp\left[-\left(\frac{z' - z}{H}\right)\right] \quad (37)$$

The value of W(z') decreases exponentially with altitude. Since y has a value of 1/2 when $z = \eta$, Eq. (37) should be a good approximation for all horizon altitudes above the inflection altitude η.

Thus, the normalized weighting function describing the total contribution from each altitude for an isothermal atmosphere is exponential with altitude above the horizon and, for altitudes above the inflection altitude, is independent of the altitude of the horizon.

Finally, by substituting Eq. (30) into Eq. (10), the radiance profile is obtained for gray atmospheres.

$$N = B\left\{1 - \exp\left[-\exp - \left(\frac{z - \eta}{H}\right)\right]\right\} \tag{38}$$

Thus, Eq. (38) is the desired expression for radiance at the limb of a planet with an isothermal atmosphere.

1.3 Error Function Transmission

Another transmission function of interest, especially in the 15-μ CO_2 absorption band, is the error function transmission which is the strong-line limit to the Elsasser integral (ref. 6) for an absorption model consisting of an infinite array of Lorentz lines of equal strength and spaced at equal intervals

$$\tau = 1 - \operatorname{erf}\left(\frac{\beta^2 x'}{2}\right)^{1/2} \tag{39}$$

where

$$\frac{\beta^2 x'}{2} = \frac{\pi \alpha S u}{d^2} \tag{40}$$

and

α = half-width of each line
S = line strength
d = line separation

The half-width α is given as a function of temperature and pressure by

$$\alpha = \alpha_o \frac{P}{P_o}\left(\frac{T_o}{T}\right)^{1/2} \tag{41}$$

where

α_o = half-width
P = pressure
T = temperature

Since this discussion concerns an isothermal atmosphere, α is given by

$$\alpha = \alpha_o P/P_o \tag{42}$$

The expression for transmission then becomes the following:

$$\tau = 1 - \operatorname{erf}\left[\frac{\pi \alpha_o S}{d^2}(\overline{uP})\right]^{1/2} \tag{43}$$

From the Curtis-Godson approximation (ref. 4) for slant paths through an isothermal atmosphere, $\overline{uP}$ is given by the following expression:

$$\overline{uP} = \int_o^u P \, d\, u \tag{44}$$

From Eq. (3), $d\, u$ is given by

$$d\, u = w\rho \, ds \tag{45}$$

Equation (44) then becomes

$$\overline{uP} = \int_o^{s(u)} w \, P\rho \, ds \tag{46}$$

For a uniformly mixed gas in an isothermal atmosphere, Eq. (11) expresses density ρ as a function of z, and pressure is given by the corresponding relationship,

$$P = P_o \exp(-z/H) \tag{47}$$

Equation (15) can again be used for ds as a function of z. By the previous argument of symmetry, the value of $\overline{uP}$ through the atmosphere is twice the value from the tangent altitude through the atmosphere. Thus, the following expression is used to calculate $\overline{uP}$:

$$\overline{uP} = 2w \int_z^\infty \frac{P_o \rho_o \exp(-2z'/H) R_e \, dz'}{\sqrt{2R_e (z' - z)}} \tag{48}$$

or

$$\overline{uP} = \sqrt{2R_e} P_o \rho_o w \int_z^\infty \frac{\exp(-2z'/H) \, dz'}{\sqrt{z' - z}} \tag{49}$$

Making the change of variable to $r = z' - z$, the following expression results:

$$\overline{uP} = \sqrt{2R_e}\, P_o\, \rho_o\, w \int_o^\infty \frac{\exp\,[-2\,(r + z)/H]\, dr}{\sqrt{r}} \tag{50}$$

Substituting the value of the definite integral, $\sqrt{\pi H/2}\, \exp\,(-2z/H)$ into Eq. (48) yields

$$\overline{uP} = \sqrt{2\pi\, R_e\, H}\, \frac{P_o\, \rho_o\, w}{\sqrt{2}}\, \exp\,(-2z/H) \tag{51}$$

The expression for transmission, Eq. (43) becomes the following:

$$\tau = 1 - \operatorname{erf}\left[\frac{\pi\alpha_o}{d^2}\, S\, \sqrt{2\pi\, R_e\, H}\, \frac{P_o\, \rho_o\, w}{\sqrt{2}}\, \exp\,(-2z/H)\right]^{1/2} \tag{52}$$

This expression can be rewritten in a form to indicate the significance of each factor, as follows:

$$\tau = 1 - \operatorname{erf}\left[\sqrt{\frac{2\pi\, R_e}{H}}\, \frac{\sqrt{2}}{4}\, \beta_o^2\, x'_o\, P_o\, \rho_o\, w\, H\, \exp\,(-2z/H)\right]^{1/2} \tag{53}$$

where

$$\beta_o^2\, x'_o = \frac{2\pi\, \alpha_o\, S}{d^2} \tag{54}$$

Equation (53) can now be written in the following form:

$$\tau = 1 - \operatorname{erf}\left\{\exp\left[-\,(z - \eta_e)/H\right]\right\} \tag{55}$$

where

$$\eta_e = \frac{H}{2}\left[G + \ell n\, \tau_e\right] \tag{56}$$

$$\tau_e = \frac{\sqrt{2}}{4}\, \beta_o^2\, x'_o\, \rho_o\, w\, P_o\, H \tag{57}$$

The expression for τ_e is similar to that for τ_o for the exponential case. The $\beta_o^2 x_o$ factor is an absorption coefficient and the extra factor P_o occurs because of the dependence of absorption on pressure. Because of the factor of two in Eq. (56), the properties of the atmosphere given in τ_e are much more important for the same value of η than for the gray atmosphere. The radiance profile for the error function transmission is given by

$$N_{\Delta\nu} = B_{\Delta\nu} \operatorname{erf}\left\{\exp\left[-(z - \eta_e)/H\right]\right\} \tag{58}$$

Equation (58) is valid only for the narrow band of frequency $\Delta\nu$ for which the constants $\beta_o^2 x_o$ is determined. For practical instrumental bandwidths, Eq. (58) must be integrated with respect to frequency. The resulting integral can not be solved in closed form and, therefore, is not very useful in understanding the radiation limb. Substituting Eq. (56) into Eq. (58), the error function profile can be written

$$N_{\Delta\nu} = B_\nu \operatorname{erf}\left[\sqrt{\tau_e} \exp\left(-\frac{z}{H} + \frac{G}{2}\right)\right] \tag{59}$$

The absorption coefficient is contained in τ_e. Over the spectral interval $14-16\mu$, the generalized absorption coefficients (ref. 7) can be fitted by an exponential with frequency. Then τ_e is given by

$$\tau_e = C_1 \exp\left(\frac{-|\nu - \nu_o|}{\gamma}\right) \tag{60}$$

where ν_o is the center of the 15μ band, and C_1 is the peak value for τ_e.

Integrating Eq. (60) over frequency (ref. 8) yields

$$N_{\Delta\nu} = \int_{\nu_1}^{\nu_2} B_\nu \operatorname{erf}\left[\exp\left(-\frac{z}{H} + \frac{G}{2}\right)\sqrt{C_1} \exp\left(\frac{-|\nu - \nu_o|}{2\gamma}\right)\right] d\nu \tag{61}$$

For normal atmospheric temperatures, 15μ is near the peak of the Planck blackbody radiance and is approximately constant over the $14-16\mu$ wavelength interval. For a symmetric bandwidth $\Delta\nu$ about ν_o, Eq. (61) becomes

$$N_{\Delta\nu} = 4 B_{\nu_o} \int_{K\sqrt{C_1}}^{K\sqrt{C_1} \exp\left(-\frac{\Delta\nu}{4\gamma}\right)} \frac{\operatorname{erf}(y)\, dy}{y} \tag{62}$$

where

$$K = \exp\left(-\frac{z}{H} + \frac{G}{2}\right) \tag{63}$$

Equation (62) must be computed numerically to give $N_{\Delta\nu}$ as a function of z. The limits for large and small values of z are easily evaluated. When z is small, K is large and $\mathrm{erf}(y)$ can be considered to be unity for all values of y in the range of integration. In this case, as expected

$$N_{\Delta\nu} = B_{\nu_o} \Delta\nu \tag{64}$$

High on the limb, z is large and K is small. The value of y is small in the range of integration requiring only the first term in

$$\mathrm{erf}(X) = \frac{2}{\sqrt{\pi}} \sum_{n=0}^{\infty} \frac{(-1)^n x^{2n+1}}{(2n+1)n!} \tag{65}$$

Upon integrating Eq. (62)

$$N_{\Delta\nu} = B_{\nu_o} \exp\left(-\frac{z}{H} + \frac{G}{2}\right) \frac{(8\gamma\sqrt{C_1})}{\sqrt{\pi}} \left[1 - \exp\left(-\frac{\Delta\nu}{4\gamma}\right)\right] \tag{66}$$

By comparison, the gray atmosphere has a constant absorption coefficient with frequency and is easily integrated to yield

$$N_{\Delta\nu} = B_{\nu_o} \Delta\nu \left\{1 - \exp\left[-\exp - \left(\frac{z-\eta}{H}\right)\right]\right\} \tag{67}$$

When the atmosphere is optically thin, $\frac{z-\eta}{H} >> 1$

$$N_{\Delta\nu} = B_{\nu_o} \Delta\nu \exp\left[-\left(\frac{z-\eta}{H}\right)\right] \tag{68}$$

For these two wideband profiles to coincide at high altitudes

$$\exp\left(\frac{\eta}{H}\right) \Delta\nu = \exp\left(\frac{G}{2}\right) \frac{(8\gamma\sqrt{C_1})}{\sqrt{\pi}} \left[1 - \exp\left(\frac{\Delta\nu}{4\gamma}\right)\right] \tag{69}$$

Now η is given by

$$\eta = H\left[G + \ell n\,(k_{abs}\, H)\right] \tag{70}$$

Solving for k_{abs} from Eqs. (69) and (70), the mean absorption coefficient

$$k = \exp\left(-\frac{G}{2}\right)\frac{(8\gamma\sqrt{C_1})}{\rho_o H\sqrt{\pi}}\left[\frac{1 - \exp\left(-\frac{\Delta\nu}{4\gamma}\right)}{\Delta\nu}\right] \tag{71}$$

The following values give a good fit to the absorption coefficients over the $14-16\mu$ spectral interval and also cause the integrated error function to approximate the gray atmosphere:

$$C_1 = 556.1$$

$$\gamma = 8.5 \text{ cm}^{-1}$$

$$\Delta\nu = 89.29 \text{ cm}^{-1}$$

$$H = 7.28 \text{ km}$$

$$G = 4.31$$

$$\rho_o = 1.41 \times 10^3 \text{ gm/m}^3$$

Inserting these values in Eq. (71) yields

$$k_{abs} = 0.000370$$

This is a reasonable value for the mean absorption coefficient for the optically thin region of the atmosphere.

1.4 Goody Model Transmission

Transmission in the water vapor bands is also of interest, and the radiance profiles for the two limiting cases of the Goody statistical model (ref. 4) can be derived. Transmission as calculated by the Goody model, is given by

$$\tau = \exp\left[\frac{-\beta x'}{\sqrt{1 + 2x'}}\right] \tag{72}$$

where

$$\left.\begin{aligned} \beta &= 2\pi\,\alpha/d \\ x' &= Su/2\pi\alpha \end{aligned}\right\} \tag{73}$$

For small x (large P), x is much smaller than 1, and the following expression for τ results:

$$\tau = \exp(-\beta x') \tag{74}$$

Using Eq. (73), the transmission can be written in the following form:

$$\tau = \exp(-su/d) \tag{75}$$

This is the same as the gray atmosphere, where

$$k_{abs} = \frac{s}{d} \tag{76}$$

The other limiting case is for x much larger than unity low pressure. The transmission can be written in the following form:

$$\tau = \exp\left[-\left(\frac{1}{2}\beta^2 x'\right)^{1/2}\right] \tag{77}$$

The error function transmission also involved the use of the factor $\sqrt{(\beta^2 x)/2}$. From the results of that calculation, the transmission can be written as follows:

$$\tau = \exp\left\{-\exp\left[-(z - \eta_e)/H\right]\right\} \tag{78}$$

where η_e is given by Eq. (56).

The radiance profile is then given by the following expression:

$$N_{\Delta\nu} = B_{\Delta\nu}\left(1 - \exp\left\{-\exp\left[-(z - \eta_e)/H\right]\right\}\right) \tag{79}$$

This equation is seen to have the same form as the radiance profile for the gray atmosphere, Eq. 38, although the constant η_e differs from η for the gray atmosphere.

1.5 Comparison of Limb Radiance Profiles for Exponential and Error Function Transmissivity Models

Since the two forms of the theoretical radiance profiles calculated here follow the general form of actual profiles, a discussion of the geometrical properties of these two profiles is of interest. The two limiting cases will be discussed first. As z approaches zero, the quantity $\exp[-(z - \eta)/H]$ approaches $\exp(\eta/H)$, which is a large positive number. The exponential radiance profile then assumes the following form:

$$N_{\Delta\nu} = B_{\Delta\nu}\left\{1 - \exp\left[\exp(\eta/H)\right]\right\} \tag{80}$$

Since $\exp(\eta/H)$ is a large number, the exponential term can be ignored, and $N_{\Delta\nu}$ approaches $B_{\Delta\nu}$. When the error function profile, Eq. (58), is examined for small z, it is found that $N_{\Delta\nu}$ also approaches $B_{\Delta\nu}$, since the error function of a large number is very close to 1. Therefore, both profiles exhibit the same value in the limiting case of small z.

The other limiting case is for large z. As z becomes large, $\exp[-(z-\eta)/H]$ becomes very small. The exponential of a small number x can be approximated by $1 + x$. Hence, for large z, Eq. (79) can be approximated as follows:

$$N_{\Delta\nu} = B_{\Delta\nu}\left(1 - \left\{1 - \exp\left[-(z - \eta_e)/H\right]\right\}\right) \tag{81}$$

or

$$N_{\Delta\nu} = B_{\Delta\nu} \exp\left[-(z - \eta_e)/H\right] \tag{82}$$

The exponential profile approaches an exponential falloff, which is characteristic of actual profiles.

Taking the first term in Eq. (65), $\mathrm{erf}(x)$ is approximated by $2/\sqrt{\pi}x$. For large z, the error function profile, Eq. (58), approaches

$$N_{\Delta\nu} = B_{\Delta\nu}\frac{2}{\sqrt{\pi}} \exp\left[-(z - \eta_e)/H\right] \tag{83}$$

A comparison of Eqs. (82) and (83) shows the same exponential decay, but a difference of a factor of $2/\sqrt{\pi}$. Both profiles exhibit the same form for both large and small z.

A comparison of the inflection points,

$$\frac{d^2 N_{\Delta\nu}}{dz^2} = 0$$

for both profiles is of interest. Differentiating the radiance profile for the exponential transmission yields

$$\frac{d N_{\Delta\nu}}{dz} = \frac{-B_{\Delta\nu}}{H} \exp\left[-(z - \eta)/H\right] \exp\left[-\exp - (z - \eta)/H\right] \tag{84}$$

This expression gives the slope at any altitude z. Differentiating again with respect to z gives

$$\frac{d^2 N_{\Delta\nu}}{dz^2} = \frac{-B_{\Delta\nu}}{H^2} \exp\left[-(z-\eta)/H\right]\left\{\exp\left[-(z-\eta)/H\right] - 1\right\} \exp\left\{-\exp\left[-(z-\eta)/H\right]\right\} \tag{85}$$

The inflection point occurs when the quantity within the brackets is zero, or $z = \eta$. This was first described by King (ref. 5). This important result states that the inflection altitude for the gray atmosphere is given simply by η, and the value of $N_{\Delta\nu}$ at this altitude is $1 - \exp(-1)$ (or approximately 0.63) of the peak value.

The slope at the inflection point is given by

$$\left.\frac{d N_{\Delta\nu}}{dz}\right|_{\eta} = \frac{-B_{\Delta\nu}}{H} \exp(-1) \tag{86}$$

or

$$\left.\frac{d N_{\Delta\nu}}{dz}\right|_{\eta} = -0.368 \frac{B_{\Delta\nu}}{H} \tag{87}$$

This equation states that the slope at the inflection point depends solely upon temperature; and, clearly, the temperature of an isothermal atmosphere is uniquely determined by the normalized slope.

A similar analysis can be performed for the error function profile. The error function of $y(x)$ is defined by

$$\operatorname{erf} y(x) = \frac{2}{\sqrt{\pi}} \int_0^{y(x)} \exp(-t^2)\, dt \tag{88}$$

The derivative of the error function is then the following expression:

$$\frac{d\left[\operatorname{erf} y(x)\right]}{dx} = \frac{2}{\sqrt{\pi}} \exp(-y^2) \frac{dy(x)}{dx} \tag{89}$$

Differentiating the radiance profile for the error function transmission, Eq. (58) yields

$$\frac{d\,N_{\Delta\nu}}{dz} = \frac{-B_{\Delta\nu}}{H}\,\frac{2}{\sqrt{\pi}}\,\exp\left[-(z-\eta_e)/H\right]\exp\left\{-\exp\left[-2(z-\eta_e)/H\right]\right\} \tag{90}$$

Differentiating again with respect to z gives

$$\frac{d^2 N_{\Delta\nu}}{dz^2} = \frac{-B_{\Delta\nu}}{H^2}\,\frac{2}{\sqrt{\pi}}\exp\left[-(z-\eta_e)/H\right]\left\{2\exp\left[-2(z-\eta_e)/H\right]-1\right\}$$

$$\exp\left\{-\exp\left[-2(z-\eta_e)/H\right]\right\} \tag{91}$$

The inflection point occurs when the quantity within the brackets is zero. Hence, the inflection altitude η must satisfy the following equation:

$$\exp\left[-2\,(\eta-\eta_e)/H\right] = \frac{1}{2} \tag{92}$$

Solving Eq. (79) for z_i yields

$$\begin{aligned}\eta &= \eta_e + \frac{H}{2}\ell n\,2\\ &= \frac{H}{2}(G + \ell n\,2\,\tau_e)\end{aligned} \tag{93}$$

This result states that the inflection altitude is typically 2 or 3 kilometers greater than η_e, and the value of $N_{\Delta\nu}$ at this altitude is erf $[\exp(-1/2\,\ell n\,2)]$, or approximately 0.68 of the peak value.

The slope at the inflection altitude is given by

$$\left.\frac{d\,N_{\Delta\nu}}{dz}\right|_{\eta} = \frac{-B_{\Delta\nu}}{H}\,\frac{2}{\sqrt{\pi}}\exp(-\ell n\,\sqrt{2})\exp\left[-\exp(-\ell n\,2)\right] \tag{94}$$

or

$$\left.\frac{d\,N_{\Delta\nu}}{dz}\right|_{\eta} = -0.4840\,\frac{B_{\Delta\nu}}{H} \tag{95}$$

The slope at the inflection altitude is again solely proportional to temperature, and the temperature is uniquely determined by the normalized slope.

Figure 5 is a plot of the normalized radiance profiles for the two cases discussed. A 200°K isothermal atmosphere has been assumed. The constants were selected to give the same asymptotic limit for large values of altitude. The circles are computed results for the 14−16μ spectral interval with an error function transmissivity model (ref. 9).* This demonstrates, as was found in subsection 1.3, that when the atmosphere is optically thin a mean absorption coefficient for a particular spectral interval may be assumed and the atmosphere may be treated as being gray. Furthermore, when the error function is integrated over frequency, the result is better approximated by the double exponential. For this reason, the gray model can be used to develop an inversion equation for wide spectral band radiance data.

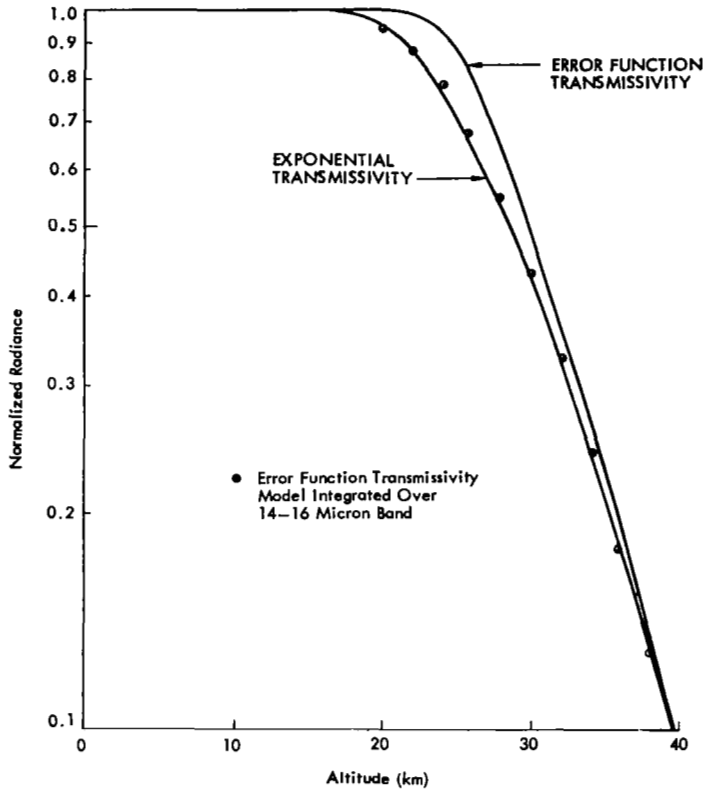

Fig. 5 Normalized Radiance Profiles for a 200°K Isothermal Atmosphere

1.6 Linearized Limb Radiance Profiles

It has already been shown in Eqs. (4) and (6) that an important parameter is the reduced absorber mass ($u/w\rho_o H$). From Eq. (25), we can write

*This reference does not give limb radiance profiles for isothermal atmospheres but outlines the numerical procedure used to solve the equation of radiative transfer.

$$\ell n\left(\frac{1}{w\rho_o}\frac{u}{H}\right) = G - x \tag{96}$$

which states that the logarithm of the mass of absorber per unit area reduced to standard condition is given by the difference between King's planetary thermal constant and the thermal equivalent altitude.

From Eqs. (4) and (10), the normalized radiance is found to be

$$\frac{N}{B} = 1 - \exp\left[-\tau_o\left(\frac{1}{w\rho_o}\right)\right] \quad \left(\frac{1}{w\rho_o}\frac{u}{H}\right) \tag{97}$$

from which

$$\left(\frac{1}{w\rho_o}\frac{u}{H}\right) = -\frac{1}{\tau_o}\ell n\left(1 - \frac{N}{B}\right) \tag{98}$$

There are two interesting results of this expression. First, when the atmosphere is optically thin $(N/B << 1)$, we find that

$$\left(\frac{1}{w\rho_o}\frac{u}{H}\right) = \frac{1}{\tau_o}\left(\frac{N}{B}\right) \tag{99}$$

which demonstrates a linear relationship between the normalized radiance and the reduced absorber mass. Second, by taking the logarithm of both sides of Eq. (98) and substituting into Eq. (96), we find that

$$\ell n\left[-\frac{1}{\tau_o}\ell n\left(1 - \frac{N}{B}\right)\right] = G - x \tag{100}$$

Thus, for isothermal atmospheres, Eq. (100) represents the linearized limb radiance profile. Since the planetary thermal constant and the optical thickness are functions of temperature, it is appropriate to normalize to a reference temperature, T_a. It is also helpful if the optical thickness is a constant, corresponding to a reference density. If surface pressure is assumed constant, the resulting linear limb radiance equation is given by,

$$G_a - x = \ell n\left[-\frac{1}{\tau_o(T_a)}\sqrt{\frac{T}{T_a}}\ell n\left(1 - \frac{N}{B}\right)\right] \tag{101}$$

This expression is plotted in fig. 6. The slope is unity with a value of planetary thermal constant G_a of 4.303 for a reference temperature of 250°K.

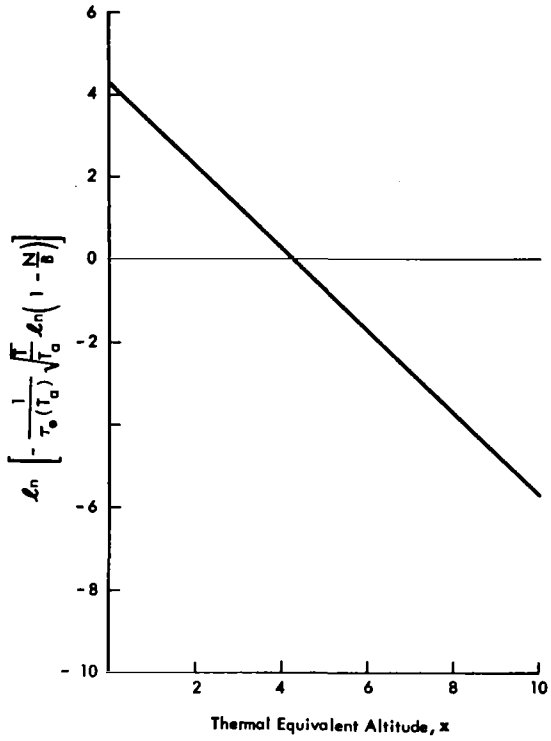

Fig. 6 Linearized Limb Radiance for Isothermal Atmospheres

If the radiance ratio N/B is measured as a function of geometric altitude z, it is clear that the temperature at altitude z can be found by rearranging Eq. (101).

$$T = \frac{z\, mg/k}{G_a - \ell n \left[- \frac{1}{\tau_o (T_a)} \sqrt{\frac{T}{T_a}}\, \ell n \left(1 - \frac{N(z)}{N(o)} \right) \right]} \tag{102}$$

However, the value of temperature on the right-hand side can only be an estimate, resulting in an error in the inferred temperature. By iteration, the inferred value of temperature can be improved. Clearly, the solution for temperature is unique, and convergence should be rapid because the dependency of the inferred temperature on the knowledge of temperature is by the logarithm of the square root of T.

Let T_i be the inferred temperature after the ith iteration. The error is given by

$$T_i - T = \frac{z\ mg/k}{G_a - \ell n \left[+ \frac{1}{\tau_o (T_a)} \sqrt{\frac{T_i - 1}{T_a}} \ell n \left(1 - \frac{N(z)}{N(o)} \right) \right]} - \frac{z\ mg/k}{G_a - \ell n \left[- \frac{1}{\tau_o (T_a)} \sqrt{\frac{T}{T_a}} \ell n \left(1 - \frac{N(z)}{N(o)} \right) \right]} \quad (103)$$

By rearranging and substituting

$$T_i - T = \frac{T}{x_i} \left\{ \ell n \left[- \frac{1}{\tau_o (T_a)} \sqrt{\frac{T_{i-1}}{T_a}} \ell n \left(1 - \frac{N}{B} \right) \right] - \ell n \left[- \frac{1}{\tau_o (T_a)} \sqrt{\frac{T}{T_a}} \ell n \left(1 - \frac{N}{B} \right) \right] \right\} \quad (104)$$

from which

$$T_i - T = \frac{T}{x_i} \left\{ \ell n \left(\frac{T_{i-1}}{T} \right)^{1/2} \right\} = \delta_i \quad (105)$$

and

$$\delta_i = \frac{T}{x_i} \left\{ \ell n \left(\frac{T + \delta_{i-1}}{T} \right)^{1/2} \right\} \quad (106)$$

Assuming that $\delta_{i-1}/T \ll 1$

$$\delta_i = \frac{1}{2x_i} \delta_{i-1} \quad (107)$$

or

$$\frac{\delta_i}{\delta_{i-1}} = \frac{1}{2x_i} \quad (108)$$

Since for the region above the middle stratosphere the thermal equivalent altitude is greater than four, the solution converges rapidly with approximately an order of magnitude improvement with each iteration. For atmospheric temperature, no more than two iterations should ever be required.

Before testing the validity of this inversion technique on an isothermal atmosphere, it is necessary to know the value of the mean absorption coefficient. From subsection 1.3, we know that the coefficient should be constant in the region where the limb is optically thin. However, since the gray model with a mean absorption coefficient is only an approximation for broad spectral bandwidths, it is to be expected that the coefficient contained in τ_o, if calculated by rewriting Eq. (101), will depart from a constant value.

Equation (101) was written to solve for k and the results are shown in fig. 7 for 200°K, 250°K, and 300°K isothermal atmospheres. As expected, the coefficients are nearly constant high on the limb above approximately 45 km for a 200°K atmosphere and rise as the gray model departs from the exact solution. The value of 0.000340 is in very good agreement with the theoretical value of 0.000370 calculated from generalized Elsasser coefficients in subsection 1.3. This demonstrates that the empirical and theoretical results are consistent.

There is also a temperature dependency of approximately 0.00000025 per °K. By using these values for the mean absorption coefficient in the calculation of $\tau_o(T_a)$ in Eq. (102), we have corrected the model and should have an exact fit of the estimated temperature to the true temperature.

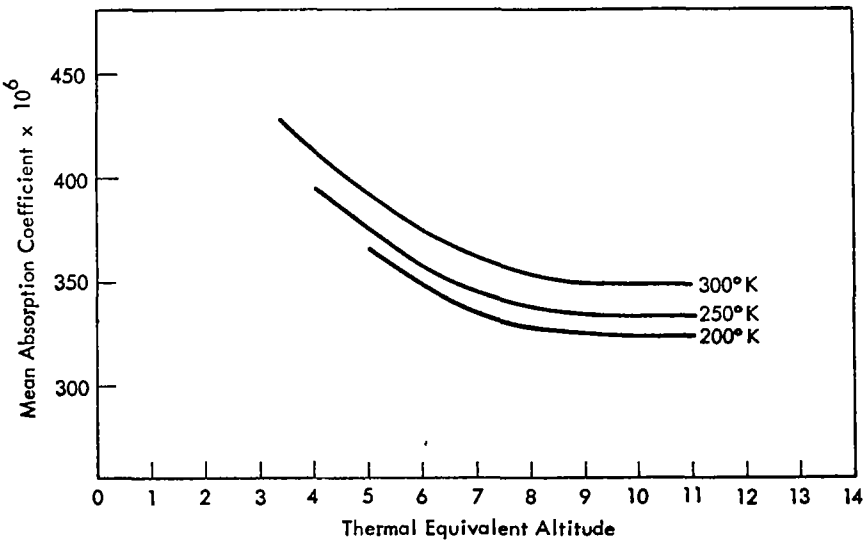

Fig. 7 Calculated Mean Absorption Coefficients for 200°, 250°, and 300°K Isothermal Atmospheres

Equation (102) was programmed to test that this inversion technique is indeed convergent and behaves as anticipated in the preceding paragraphs. Computed radiance data for a 200°K isothermal atmosphere was used with an initial estimate of 220°K.* The results are given in Table 1. The first estimate of temperature reduces the error in the initial estimate by approximately an order of magnitude as expected, although the residual errors do not follow Eq. (108) precisely. The relative error between successive iterations does behave according to Eq. (108), and the solution has converged with an average relative error of 0.1°K, which is smaller than the least significant digit in temperature (1°K).

TABLE 1

INFERRED TEMPERATURES FOR A 200°K ISOTHERMAL ATMOSPHERE

Initial Estimate -220°K, Error = +20°K

Altitude (km)	1st			2nd			3rd		
	Temperature (°K)	Error		Temperature (°K)	Error		Temperature (°K)	Error	
		$T_i - T$	$T_{i-1} - T_i$		$T_i - T$	$T_{i-1} - T_i$		$T_i - T$	$T_{i-1} - T_i$
30	202.4	2.4	17.6	200.8	0.8	1.6	200.6	0.6	0.2
32	202.3	2.3	17.7	200.7	0.7	1.6	200.6	0.6	0.1
34	202.0	2.0	18.0	200.5	0.5	1.5	200.4	0.4	0.1
36	201.7	1.7	18.3	200.3	0.3	1.4	200.2	0.2	0.1
38	201.5	1.5	18.5	200.1	0.1	1.4	200.0	0.0	0.1
40	201.3	1.3	18.7	200.0	0.0	1.3	199.9	-0.1	0.1
42	201.2	1.2	18.8	200.0	0.0	1.2	199.9	-0.1	0.1
44	201.2	1.2	18.8	200.0	0.0	1.2	200.0	0.0	0.0
46	201.0	1.0	19.0	199.9	-0.1	1.1	199.8	-0.2	0.1
48	200.9	0.9	19.1	199.8	-0.2	1.1	199.7	-0.3	0.1
50	200.8	0.8	19.2	199.7	-0.3	1.1	199.6	-0.4	0.1
52	200.7	0.7	19.3	199.7	-0.3	1.0	199.7	-0.3	0.0
54	200.7	0.7	19.3	199.7	-0.3	1.0	199.7	-0.3	0.0
56	200.6	0.6	19.4	199.7	-0.3	0.9	199.7	-0.3	0.0
58	200.6	0.6	19.4	199.7	-0.3	0.9	199.6	-0.4	0.1
60	200.6	0.6	19.4	199.7	-0.3	0.9	199.6	-0.4	0.1
Average	201.2	1.2	18.8	200.0	0.0	1.2	199.9	-0.1	0.1

*See footnote on p. 21

SECTION 2. – LINEAR TEMPERATURE GRADIENT ATMOSPHERES

2.1 Positive Temperature Gradient

In this section, the closed form solution of the equation of radiative transfer will be found for an atmosphere with a linear temperature gradient $L = dT/dz$. The meteorological term lapse rate, the negative of the temperature gradient, will not be used in this discussion.

From the hydrostatic equation and the equation of state

$$\frac{d\rho}{\rho} = - \frac{mg}{kT} dz - \frac{dT}{T} \tag{109}$$

For a linear temperature gradient

$$T = T_o + L (z - z_o) \tag{110}$$

Equation (96) becomes

$$\frac{d\rho}{\rho} = - \frac{mg\, dz}{k \left[T_o + L (z - z_o)\right]} - \frac{dT}{T} \tag{111}$$

Integrating this equation yields

$$\rho = \rho_o \left[\frac{1}{1 + \dfrac{L (z - z_o)}{T_o}} \right]^{T_o/(H_o L)+1} \tag{112}$$

where H_o is the scale height at temperature T_o. The exponent is independent of temperature since H is proportional to temperature. In the limit as $L \to 0$, Eq. (11) results.

At an altitude z', the value of u_s for ℓ positive and with a positive, constant L above the horizon altitude z, is obtained by substitution of Eq. (112) into Eq. (16).

$$u_s = \int_{\infty}^{z'} w\rho_z \left[\frac{1}{1 + \frac{L_z}{T_z}(z'' - z)} \right]^{T_z/(H_z L_z)+1} \frac{(-R_e)\, dz''}{\sqrt{2 R_e (z'' - z)}} \tag{113}$$

or

$$u_s = \frac{1}{2}\sqrt{2R_e}\, w\rho_z \int_{z'}^{\infty} \frac{dz''\,(z'' - z)^{-1/2}}{\left[1 + \frac{L_z}{T_z}(z'' - z)\right]^{T_z/(H_z L_z)+1}} \tag{114}$$

Defining the scale height gradient γ by

$$\gamma_z = \frac{L_z H_z}{T_z} = \frac{k L_z}{mg} \tag{115}$$

Equation (114) becomes

$$u_s = \frac{1}{2}\sqrt{2 R_e}\, w\rho_z \int_{z'}^{\infty} \frac{dz''\,(z'' - z)^{-1/2}}{\left[1 + \gamma_z \left(\frac{z'' - z}{H_z}\right)\right]^{1/\gamma_z + 1}} \tag{116}$$

With the change of variable

$$t = \frac{\gamma_z (z'' - z)/H_z}{1 + \gamma_z (z'' - z)/H_z} \tag{117}$$

Equation (116) becomes

$$u_s = \frac{1}{2}\sqrt{2 R_e H_z}\,\frac{w\rho_z}{\sqrt{\gamma_z}}\left[\int_0^1 t^{-1/2}\,(1 - t)^{1/\gamma_z - 1/2}\,dt - \int_0^y t^{-1/2}\,(1 - t)^{1/\gamma_z - 1/2}\,dt\right] \tag{118}$$

where

$$y = \left[\gamma_z\,(z' - z)/H_z\right]\Big/\left[1 + \gamma_z(z' - z)/H_z\right] \tag{119}$$

The first integral is the beta function $B\,(m, n)$, defined by

$$B\,(m, n) = \int_0^1 t^{m-1}\,(1 - t)^{n-1}\,dt \tag{120}$$

It can be shown (ref. 10) that

$$B\,(m, n) = \frac{\Gamma\,(m)\,\Gamma\,(n)}{\Gamma\,(m + n)} \tag{121}$$

where $\Gamma\,(x)$ is the gamma function. Equation (105) then becomes, $\Gamma\,(1/2) = \sqrt{\pi}$,

$$u_s = \frac{1}{2}\sqrt{2\pi R_e H_z}\,\frac{w\rho_z}{\sqrt{\gamma_z}}\,\frac{\Gamma\,(1/\gamma_z + 1/2)}{\Gamma\,(1/\gamma_z + 1)}$$

$$\left[1 - \frac{\Gamma\,(1/\gamma_z + 1)}{\sqrt{\pi}\,\Gamma\,(1/\gamma_z + 1/2)}\int_0^y t^{-1/2}\,(1 - t)^{1/\gamma_z - 1/2}\,dt\right] \tag{122}$$

The integral remaining is the incomplete beta function, $B_x\,(m, n)$, defined by (ref. 3)

$$B_x\,(m, n) = \int_0^x t^{m-1}\,(1 - t)^{n-1}\,dt \tag{123}$$

The incomplete beta function ratio is defined by

$$I_x\,(m, n) = B_x\,(m, n)/B\,(m, n) \tag{124}$$

and has several important statistical applications. Tabulated values of this function can be found in ref. 10.

With this definition, Eq. (122) can be rewritten as

$$u_s = \frac{1}{2}\sqrt{2\pi R_e H_z}\,\frac{w\rho_z}{\sqrt{\gamma_z}}\,\frac{\Gamma(1/\gamma_z + 1/2)}{\Gamma(1/\gamma_z + 1)}\left[1 - I_y(1/2,\, 1/\gamma_z + 1/2)\right] \tag{125}$$

Similarly for negative ℓ again with L a positive constant

$$u_s = \frac{1}{2}\sqrt{2\pi R_e H_z}\,\frac{w\rho_z}{\sqrt{\gamma_z}}\,\frac{\Gamma(1/\gamma_z + 1/2)}{\Gamma(1/\gamma_z + 1)}\left[1 + I_y(1/2,\, 1/\gamma_z + 1/2)\right] \tag{126}$$

Stirling's formula states that

$$\Gamma(x) \cong e^{-x} x^x \sqrt{\frac{2\pi}{x}} \tag{127}$$

Using this approximation, Eqs. (125) and (126) become (for $\pm\ell$)

$$u_s = \frac{1}{2}\sqrt{2\pi R_e H_z}\, w\rho_z \left(\frac{e}{1+\gamma_z}\right)^{1/2} \left[\frac{1+\gamma_z/2}{1+\gamma_z}\right]^{1/\gamma_z} \left[1 \pm I_y(1/2,\, 1/\gamma_z + 1/2)\right] \tag{128}$$

From Eqs. (110) and (115)

$$H_z = H_o + \gamma_z \tag{129}$$

where $z_o = 0$, and

$$H_z = H_o\left(1 + \frac{\gamma_z}{H_o}\right) \tag{130}$$

Substituting Eqs. (112), (115), and (130) into Eq. (128) gives the absorber mass along a path s in terms of the base density and the scale height corresponding to the base temperature. Thus (for $\pm\ell$),

$$u_s = \frac{1}{2}\sqrt{2\pi R_e H_o}\,\frac{w\rho_o}{\left[1 + \frac{\gamma_z}{H_o}\right]^{1/\gamma+1/2}} \left(\frac{e}{1+\gamma}\right)^{1/2} \left(\frac{1+\gamma/2}{1+\gamma}\right)^{1/\gamma} \left[1 \pm I_y(1/2,\, 1/\gamma + 1/2)\right] \tag{131}$$

It is convenient to define $K_{1/2}(\gamma)$ by (see Appendix B)

$$K_{1/2}(\gamma) = \left(\frac{e}{1+\gamma}\right)^{1/2} \left[\frac{1+\gamma/2}{1+\gamma}\right]^{1/\gamma} \tag{132}$$

The function $K_{1/2}(\gamma)$ expresses the change in u_s due to the temperature gradient above the horizon altitude z. It has a value of unity for $\gamma = 0$.

The transmission is found by substituting Eqs. (131) and (132) into Eq. (2).

$$\tau_s = \exp - \left\{ \frac{k\sqrt{2\pi R_e H_z}}{2} w\rho_z K_{1/2}(\gamma_z) \left[1 \pm I_y (1/2, 1/\gamma_z + 1/2)\right] \right\} \tag{133}$$

Similarly, the weighting function $\frac{\partial \tau_s}{\partial s}$ is given by Eq. (7a) as

$$\frac{\partial \tau_s}{\partial s} = - \tau_s k \frac{\partial u_s}{\partial s} \tag{134}$$

From Eq. (112) $\frac{\partial u_s}{\partial s}$ is given by

$$\frac{\partial u_s}{\partial s} = w\rho_z \left[\frac{1}{1 + \gamma_z \left(\frac{z' - z}{H_z}\right)} \right]^{1/\gamma_z + 1} \tag{135}$$

and by substitution, the weighting function is given by

$$\frac{\partial \tau_s}{\partial s} = - \frac{k\, w\rho_z\, \tau_s}{\left[1 + \gamma_z \frac{(z' - z)}{H_z}\right]^{1/\gamma_z + 1}} \tag{136}$$

The equation of radiative transfer, Eq. (1), can be rewritten as

$$N_\lambda = - \int_1^{\tau(s=\infty)} B_\lambda (T)\, d\tau \tag{137}$$

For an atmosphere with a temperature gradient, $B_\lambda(T)$ is not a constant and cannot be taken outside the integral. Expanding $B_\lambda(T)$ in a Taylor series about T_o

$$B_\lambda(T) = B_\lambda(T_o) + \left.\frac{\partial B_\lambda(T)}{\partial T}\right|_{T=T_o} (T - T_o) + \left.\frac{\partial^2 B_\lambda(T)}{2!\,\partial T^2}\right|_{T=T_o} (T - T_o)^2 + \ldots \quad (138)$$

Taking the partial derivative of the Planck function with respect to temperature yields

$$\frac{\partial B_\lambda(T)}{\partial T} = \frac{B_\lambda(T)}{T} \frac{C_2/\lambda T}{1 - \exp(-C_2/\lambda T)} \quad (139)$$

For wavelengths and temperatures of interest in this study, the exponential term can be ignored and

$$\frac{1}{B_\lambda(T_o)} \left.\frac{\partial B_\lambda(T)}{\partial T}\right|_{T=T_o} = \frac{C_2}{\lambda T_o^2} \quad (140)$$

and

$$\frac{1}{B_\lambda(T_o)} \left.\frac{\partial^2 B_\lambda(T)}{\partial T^2}\right|_{T=T_o} = \frac{C_2}{\lambda T_o^2}\left(\frac{C_2}{\lambda T_o^2} - \frac{2}{T_o}\right) \quad (141)$$

Hence $B_\lambda(T)$ is given approximately by

$$B_\lambda(T) = B_\lambda(T_o)\left[1 + \frac{C_2}{\lambda T_o}\left(\frac{T - T_o}{T_o}\right) + \frac{1}{2}\frac{C_2}{\lambda T_o}\left(\frac{C_2}{\lambda T_o} - 2\right)\left(\frac{T - T_o}{T_o}\right)^2\right] \quad (142)$$

Since $T = T_o + L(z - z_o)$, $T - T_o$ is given by

$$T - T_o = L(z - z_o) \quad (143)$$

In considering the horizon problem, the value of T_o will be T_z, the temperature at the horizon. The radiance given by Eq. (1) can then be written as

$$N_\lambda = B_\lambda (T_z) \left[- \int_1^{\tau(s=\infty)} d\tau - \frac{C_2}{\lambda T_z^2} L_z \int_1^{\tau(s=\infty)} (z' - z)\, d\tau - \frac{L_z^2}{2} \frac{C_2}{\lambda T_z^2} \left(\frac{C_2}{\lambda T_z^2} - \frac{2}{T_z} \right) \int_1^{\tau(s=\infty)} (z' - z)^2 d\tau \right] \tag{144}$$

where z' is the altitude along the path of integration.

The first integral I_o is easily evaluated, yielding

$$I_o = 1 - \exp - \left[k \sqrt{2\pi R_e H_z}\, w\rho_z\, K_{1/2} (\gamma_z) \right] \tag{145}$$

Using Eq. (121), the second integral can be written in the form

$$I_1 = \frac{C_2}{\lambda T_z^2} L_z \int_o^\infty (z' - z)(-\tau_s)\, k \frac{\partial u_s}{\partial s}\, ds \tag{146}$$

where τ_s is given by Eq. (133). This integral cannot be evaluated in closed form. However τ_s can be expanded in a series, and the resulting integrals evaluated.

The incomplete beta function ratio can be expanded in the following series (ref. 10):

$$I_x (a, b) = \frac{x^a (1 - x)^b}{a\, B (a, b)} \left[1 + \sum_{n=o}^{\infty} \frac{B (a + 1, n + 1)}{B (a + b, n + 1)} x^{n+1} \right] \tag{147}$$

Only the first term need be kept in the transmission function, since x is small.

$$\tau = \exp - \left\{ \frac{k \sqrt{2\pi R_e H_z}}{2} \frac{w\rho_z}{\sqrt{\gamma_z}} \frac{\Gamma (1/\gamma_z + 1/2)}{\Gamma (1/\gamma_z + 1)} \left[1 \pm \frac{2 \sqrt{\gamma_z (z' - z)/H_z} \left(1 + \gamma_z (z' - z)/H_z\right)^{-(1/\gamma_z + 1)}}{\sqrt{\pi}\, \Gamma (1/\gamma_z + 1/2)/\Gamma (1/\gamma_z + 1)} \right] \right\} \tag{148}$$

Equation (146) is solved by expanding τ and performing the integrals. The second terms cancel by symmetry. The result is that

$$I_1 = \frac{C_2}{\lambda T_z^2} L_z \tau_z \left\{ 2 \int_z^\infty \frac{(z' - z)\, k\, w\rho_z\, R_e\, dz'}{\left[1 + \gamma_z (z' - z)/H_z\right]^{1/\gamma_z + 1} \sqrt{2 R_e (z' - z)}} \right.$$

$$\left. + 2 \int_z^\infty \frac{(z' - z)^2 \left(k\, w\rho_z\right)^3 R_e^2 R_e^2\, dz'}{\left[1 + \gamma_z (z' - z)/H_z\right]^{3(1/\gamma_z + 1)} \sqrt{2 R_e (z' - z)}} \right\} \tag{149}$$

where

$$\tau_z = \exp - \left[k \frac{\sqrt{2\pi R_e H_z}}{2} w\rho_z K_{1/2}(\gamma_z) \right] \tag{150}$$

Making the change of variable

$$r = \gamma_z (z' - z)/H_z \tag{151}$$

Equation (149) becomes

$$I_1 = \frac{C_2}{\lambda T_z^2} L_z \tau_z \left\{ k\, w\rho_z \sqrt{2 R_e} \left(\frac{H_z}{\gamma_z}\right)^{3/2} \int_0^\infty \frac{r^{1/2}\, dr}{\left(1 + r\right)^{1/\gamma_z + 1}} \right.$$

$$\left. + \frac{H_z}{\gamma_z} \left(k\, w\rho_z\right)^2 R_e \left[k\, w\rho_z \sqrt{2 R_e} \left(\frac{H_z}{\gamma_z}\right)^{3/2} \right] \int_0^\infty \frac{r^{3/2}\, dr}{\left(1 + r\right)^{3(1/\gamma_z + 1)}} \right\} \tag{152}$$

Evaluating the integrals yields the following

$$I_1 = \frac{C_2}{\lambda T_z^2} L_z \tau_z \left\{ k w \rho_z \frac{\sqrt{2\pi R_e H_z}}{2} \left(\frac{H_z}{z}\right) \frac{1}{\sqrt{\gamma_z^3}} \frac{\Gamma(1/\gamma_z - 1/2)}{\Gamma(1/\gamma_z + 1)} \right.$$

$$\left. + H_z (k w \rho_z)^2 R_e \left[k w \rho_z \frac{\sqrt{2\pi R_e H_z}}{2} \left(\frac{H_z}{z}\right) \right] \frac{1}{\sqrt{\gamma_z^5}} \left(\frac{3}{2}\right) \frac{\Gamma(3/\gamma_z + 1/2)}{\Gamma(3/\gamma_z + 3)} \right\} \quad (153)$$

Using Stirling's approximation

$$I_1 = \frac{C_2}{\lambda T_z} \gamma_z \tau_z k w \rho_z \frac{\sqrt{2\pi R_e H_z}}{2} K_{3/2}(\gamma_z) \left\{ 1 + (k w \rho_z)^2 R_e H_z \left(\frac{3}{2}\right) \frac{K'_{5/2}(\gamma_z)}{K_{3/2}(\gamma_z)} \right\} \quad (154)$$

where

$$K_{3/2}(\gamma_z) = \left(\frac{e}{1 + \gamma_z}\right)^{3/2} \left(\frac{1 - \gamma_z/2}{1 + \gamma_z}\right)^{1/\gamma_z - 1} \quad (155)$$

and

$$K'_{5/2}(\gamma_z) = \left(\frac{e}{3 + 3\gamma_z}\right)^{5/2} \left(\frac{3 + \gamma_z/2}{3 + 3\gamma_z}\right)^{3/\gamma_z} \quad (156)$$

The last term in the brackets of Eq. (154) is negligible above 25 km.

The third integral in Eq. (144) is given by

$$I_2 = \frac{C_2}{\lambda T_z^2} \left(\frac{C_2}{\lambda T_z^2} - \frac{2}{T_z}\right) L_z^2 \tau_z \left\{ k w \rho_z \frac{\sqrt{2\pi R_e H_z}}{2} \frac{3}{4} \left(\frac{H_z}{\gamma_z}\right)^2 \frac{1}{\sqrt{\gamma_z}} \frac{\Gamma(1/\gamma_z - 3/2)}{\Gamma(1/\gamma_z + 1)} \right.$$

$$\left. + (k w \rho)^2 R_e k w \rho_z \frac{\sqrt{2\pi R_e H_z}}{2} \frac{15}{8} \left(\frac{H_z}{\lambda_z}\right)^3 \frac{1}{\sqrt{\gamma_z}} \left(\frac{3}{2}\right) \frac{\Gamma(3/\gamma_z - 1/2)}{\Gamma(3/\gamma_z + 3)} \right\} \quad (157)$$

Or, using Stirling's approximation

$$I_2 = \frac{C_2}{\lambda T_z}\left(\frac{C_2}{\lambda T_z} - 2\right)\gamma_z^2\,\tau_z k w\rho_z \frac{\sqrt{2\pi R_e H_z}}{2}\frac{3}{4}K_{5/2}(\gamma_z)$$

$$\left\{1 + \left(k w\rho_z\right)^2 R_e H_z\left(\frac{5}{2}\right)\frac{K'_{7/2}(\gamma_z)}{K_{5/2}(\gamma_z)}\right\} \qquad (158)$$

where

$$K_{5/2}(\gamma_z) = \left(\frac{e}{1+\gamma_z}\right)^{5/2}\left(\frac{1 - 3\gamma_z/2}{1+\gamma_z}\right)^{1/\gamma_z - 2} \qquad (159)$$

and

$$K'_{7/2}(\gamma_z) = \left(\frac{e}{3+3\gamma_z}\right)^{7/2}\left(\frac{3 - \gamma_z/2}{3+3\gamma_z}\right)^{3/\gamma_z - 1} \qquad (160)$$

Again, the last term in the brackets of Eq. (158) is negligible above 25 km.

2.2 Negative Temperature Gradients

It is obvious that a negative temperature gradient cannot extend to infinity. The integrals will be taken from the horizon altitude to the altitude at which the temperature is zero. Temperatures near zero do not exist in a real atmosphere, but since density falls off rapidly with altitude, the error in extending the gradient to zero temperature is negligible.

For a negative temperature gradient, u_s becomes

$$u_s = \frac{\sqrt{2R_e}}{2} w\rho_z \int_{z'}^{z(T=0)} \frac{dz''\,(z'' - z)^{-1/2}}{\left[1 - (-\gamma_z)\left(\frac{z'' - z}{H_z}\right)\right]^{-1/(-\gamma_z)+1}} \qquad (161)$$

Here $(-\gamma_z)$ is a positive quantity. With the change of variable

$$r = (-\gamma_z)\left(\frac{z'' - z}{H_z}\right)$$

Equation (161) becomes

$$u_s = \frac{\sqrt{2\,R_e}}{2}\, w\,\rho_z \left[\frac{H_z}{(-\gamma_z)}\right]^{1/2} \int_{(-\gamma_z)\frac{(z'-z)}{H_z}}^{1} r^{-1/2}\left[1 - r\right]^{1/(-\gamma_z)-1} dr \qquad (162)$$

Evaluating the integral

$$u_s = \frac{\sqrt{2\pi\,R_e\,H_z}}{2}\,\frac{w\,\rho_z}{\sqrt{(-\gamma_z)}}\,\frac{\Gamma\left(1/(-\gamma_z)\right)}{\Gamma\left(1/(-\gamma_z) + 1/2\right)}\left[1 \pm I_v\left(1/2\,,\ 1/(-\gamma_z)\right)\right] \qquad (163)$$

where

$$v = (-\gamma_z)\,(z' - z)/H_z \qquad (164)$$

Using Stirling's formula

$$u_s = \frac{\sqrt{2\pi\,R_e\,H_z}}{2}\, w\rho_z K_{1/2}(-\gamma_z)\left[1 \pm I_v\left(1/2\,,\ 1/(-\gamma_z)\right)\right] \qquad (165)$$

where

$$K_{1/2}(-\gamma_z) = e^{1/2}\left[\frac{1}{1 + (-\gamma_z)/2}\right]^{1/(-\gamma_z)} \qquad (166)$$

The three integrals in Eq. (144) can also be evaluated assuming τ_s in the second integral is given by τ_z. Then,

$$I_o = 1 - \exp - \left[k\sqrt{2\pi\,R_e\,H_z}\; w\,\rho_z\,K_{1/2}(-\gamma_z)\right] \qquad (167)$$

The second integral is given by

$$I_1 = \frac{C_2}{\lambda T_z^2} L_z \tau_z k w \rho_z \frac{\sqrt{2\pi R_e H_z}}{2} \left[\frac{H_z}{(-\gamma_z)}\right] \frac{1}{\sqrt{(-\gamma_z)}} \frac{\Gamma\left(1/(-\gamma_z)\right)}{\Gamma\left(1/(-\gamma_z) + 3/2\right)} \tag{168}$$

Using Stirling's formula

$$I_1 = \frac{C_2}{\lambda T_z} \gamma_z \tau_z k w \rho_z \frac{\sqrt{2\pi R_e H_z}}{2} K_{3/2}(-\gamma_z) \tag{169}$$

where

$$K_{3/2}(-\gamma_z) = e^{3/2} \left[\frac{1}{1 + \frac{3}{2}(-\gamma_z)}\right]^{1/(-\gamma_z)+1} \tag{170}$$

Similarly, the third integral is given by

$$I_2 = \frac{C_2}{\lambda T_z^2} \left(\frac{C_2}{\lambda T_z^2} - \frac{2}{T_z}\right) \frac{L_z^2}{2} \tau_z k w \rho_z \sqrt{2\pi R_e H_z} \left(\frac{3}{4}\right) \left[\frac{H_z}{(-\gamma_z)}\right]^2 \frac{1}{\sqrt{(-\gamma_z)}} \frac{\Gamma\left(1/(-\gamma_z)\right)}{\Gamma\left(1/(-\gamma_z) + 5/2\right)} \tag{171}$$

Again, using Stirling's formula

$$I_2 = \frac{C_2}{\lambda T_z} \left(\frac{C_2}{\lambda T_z} - 2\right) \gamma_z^2 \tau_z k w \rho_z \frac{\sqrt{2\pi R_e H_z}}{2} \left(\frac{3}{4}\right) K_{5/2}(-\gamma_z) \tag{172}$$

where

$$K_{5/2}(-\gamma_z) = e^{5/2} \left[\frac{1}{1 + \frac{5}{2}(-\gamma_z)}\right]^{1/(-\gamma_z)+2} \tag{173}$$

2.3 Limb Radiance

The full expression for the radiance can now be written. The distinction between positive and negative temperature gradients will be dropped, since the appropriate function to be used is given previously. Also, the second terms in the I_1 and I_2 integrals will be ignored.

The radiance can then be written as

$$N_\lambda = B_\lambda (T_z) \left\{ 1 - \exp - \left[k \sqrt{2\pi R_e H_z}\ w \rho_z K_{1/2} (\gamma_z) \right] \right.$$

$$+ \frac{C_2}{\lambda T_z} \gamma_z \tau_z \frac{k \sqrt{2\pi R_e H_z}}{2} w \rho_z K_{3/2} (\gamma_z)$$

$$\left. + \frac{C_2}{\lambda T_z} \left(\frac{C_2}{\lambda T_z} - 2 \right) \gamma_z^2 \tau_z \frac{k \sqrt{2\pi R_e H_z}}{2} w \rho_z \frac{3}{4} K_{5/2} (\gamma_z) \right\} \qquad (174)$$

Combining the second and third terms

$$N_\lambda = B_\lambda (T_z) \left\{ 1 - \exp - \left[k \sqrt{2\pi R_e H_z}\ w \rho_z K_{1/2} (\gamma_z) \right] \right.$$

$$\left. + \frac{C_2}{\lambda T_z} \gamma_z \tau_z \frac{k \sqrt{2\pi R_e H_z}}{2} w \rho_z K_{3/2} (\gamma_z) \left[1 + \left(\frac{C_2}{\lambda T_z} - 2 \right) \gamma_z \left(\frac{3}{4} \right) \frac{K_{5/2} (\gamma_z)}{K_{3/2} (\gamma_z)} \right] \right\}$$

(175)

It is convenient to write $B_\lambda (T_z)$ in terms of $B_\lambda (T°)$, where $T°$ is the temperature that gives the radiance at $z = 0$. Equation (175) becomes

$$N_\lambda = B_\lambda (T°) \left[1 + \frac{C_2}{\lambda T°}\left(\frac{T_z - T°}{T°}\right) + \frac{1}{2}\frac{C_2}{\lambda T°}\left(\frac{C_2}{\lambda T°} - 2\right)\left(\frac{T_z - T°}{T°}\right)^2\right]$$

$$\left\{1 - \exp - \left[k\sqrt{2\pi R_e H_z}\, w \rho_z K_{1/2}(\gamma_z)\right] + \frac{C_2}{\lambda T_z}\gamma_z \tau_z \frac{k\sqrt{2\pi R_e H_z}}{2} w \rho_z K_{3/2}(\gamma_z)\right.$$

$$\left.\left[1 + \left(\frac{C_2}{\lambda T_z} - 2\right)\gamma_z \left(\frac{3}{4}\right)\frac{K_{5/2}(\gamma_z)}{K_{3/2}(\gamma_z)}\right]\right\} \qquad (176)$$

If $B_\lambda (T°)$ is interpreted as the radiance on the flat part of the limb profile, $T°$ becomes the equivalent blackbody temperature of the atmosphere. Dividing both sides of Eq. (40) by $B_\lambda (T°)$ gives the normalized limb radiance profile equation for linear temperature gradient atmospheres.

2.4 Linearized Limb Radiance Equation

Equation (176) can be linearized similar to Eq.(101) for isothermal atmospheres. First, write Eq. (176) in the form

$$N_\lambda = B_\lambda (T°)(1 + C')\left[1 - \tau (s = \infty) + B'\right] \qquad (177)$$

Solving for $\tau (s = \infty)$

$$\tau (s = \infty) = 1 - \frac{N}{(1 + C') B_\lambda (T°)} + B' \qquad (178)$$

Taking the natural logarithm of both sides,

$$\ell n\, \tau (s = \infty) = \ell n \left[1 - \frac{N}{(1 + C') B_\lambda (T°)} + B'\right] \qquad (179)$$

Now $\ell n\, \tau (s = \infty)$ is given by

$$\ell n\, \tau (s = \infty) = - k\sqrt{2\pi R_e H_z}\, w \rho_z K_{1/2}(\gamma_z) \qquad (180)$$

or

$$\ell n\, \tau\, (s = \infty) = - \sqrt{\frac{2\pi R_e}{H_z}}\, k\, H_z\, w\, \rho_z\, K_{1/2}\, (\gamma_z) \tag{181}$$

Factoring out T_z

$$\ell n\, \tau\, (s = \infty) = - \sqrt{\frac{2\pi R_e}{H_a}}\, k\, H_a\, w\, \rho_z\, K_{1/2}\, (\gamma_z)\, \sqrt{\frac{T_z}{T_a}} \tag{182}$$

where T_a is some arbitrary reference temperature. Let ρ_{ao} be the density at $z = 0$ for an isothermal atmosphere of temperature T_a, then

$$\ell n\, \tau\, (s = \infty) = - \sqrt{\frac{2\pi R_e}{H_a}}\, k\, H_a\, w\, \rho_{ao}\, \frac{w\, \rho_z}{w\, \rho_{ao}}\, K_{1/2}\, (\gamma_z)\, \sqrt{\frac{T_z}{T_z}} \tag{183}$$

Since the surface pressure is considered approximately constant for all temperatures, ρ_{ao} is the surface density scaled by the ratio T_a/T_o and Eq. (183) becomes

$$\ell n\, \tau\, (s = \infty) = - \sqrt{\frac{2\pi R_e}{H_a}}\, k\, H_a\, w\, \rho_{ao}\, \frac{\rho_z}{\rho_o}\, K_{1/2}\, (\gamma_z)\, \sqrt{\frac{T_z\, T_a}{T_o^2}} \tag{184}$$

Equation (184) can be rewritten as

$$\ell n\, \tau (s = \infty) = - \exp\, (G_a)\, \tau_o\, (T_a)\, \frac{\rho_z}{\rho_o}\, K_{1/2}\, (\gamma_z) \sqrt{\frac{T_z\, T_a}{T_o^2}} \tag{185}$$

where

$$G_a = \frac{1}{2}\, \ell n\, \frac{2\pi R_e}{H_a} \tag{186}$$

and

$$\tau_o\, (T_a) = k\, H_a\, w\, \rho_{ao} \tag{187}$$

Combining Eqs. (185) and (179) and multiplying by e^{-x}

$$- \exp (G_a - x)\, \tau_o (T_a) \frac{\rho_z}{\rho_o} K_{1/2} (\gamma_z) \sqrt{\frac{T_z T_a}{T_o^2}} = e^{-x} \ell n \left[1 - \frac{N}{(1 + C')\, B_\lambda (T°)} + B' \right] \tag{188}$$

Rearranging and taking the natural logarithm of both sides,

$$G_a - x = \ell n \left\{ - \sqrt{\frac{T_o^2}{T_z T_a}} \frac{e^{-x}}{\rho_z / \rho_o} \frac{1}{\tau_o (T_a)\, K_{1/2} (\gamma_z)} \ell n \left[1 - \frac{N}{(1 + C')\, B_\lambda (T°)} + B' \right] \right\} \tag{189}$$

Equation (189) is the linearized limb radiance equation. It is nonlinear in temperature since T appears on both sides of the equation. The ratio of exp (- x) to the density ratio differs from unity to the extent that the atmosphere varies from being isothermal. Furthermore, the ratio has a value of unity in the middle stratosphere.

The radiance values for the 120 climatological model atmospheres of ref. 9 yield values very close to the straight line described by Eq. (189) as seen in fig. 8. Real atmospheres do not have a constant temperature gradient extending to infinity. However, since most of the radiation comes from a layer a few kilometers above the horizon altitude, an equivalent γ can be used. The computer program which generated fig. 8 gave a weight of 0.6 to the temperature gradient from 0. to 2. km above the horizon, and a weight of 0.4 to the temperature gradient from 2. to 4. km above the horizon. These weights are unsatisfactory and produced much of the scatter at thermal equivalent altitudes below 7. In the remainder of this report, the exponential weighting function suggested by Eq. (37) of Section 1 was approximated by a seven-layer model, each layer being 2. km thick.

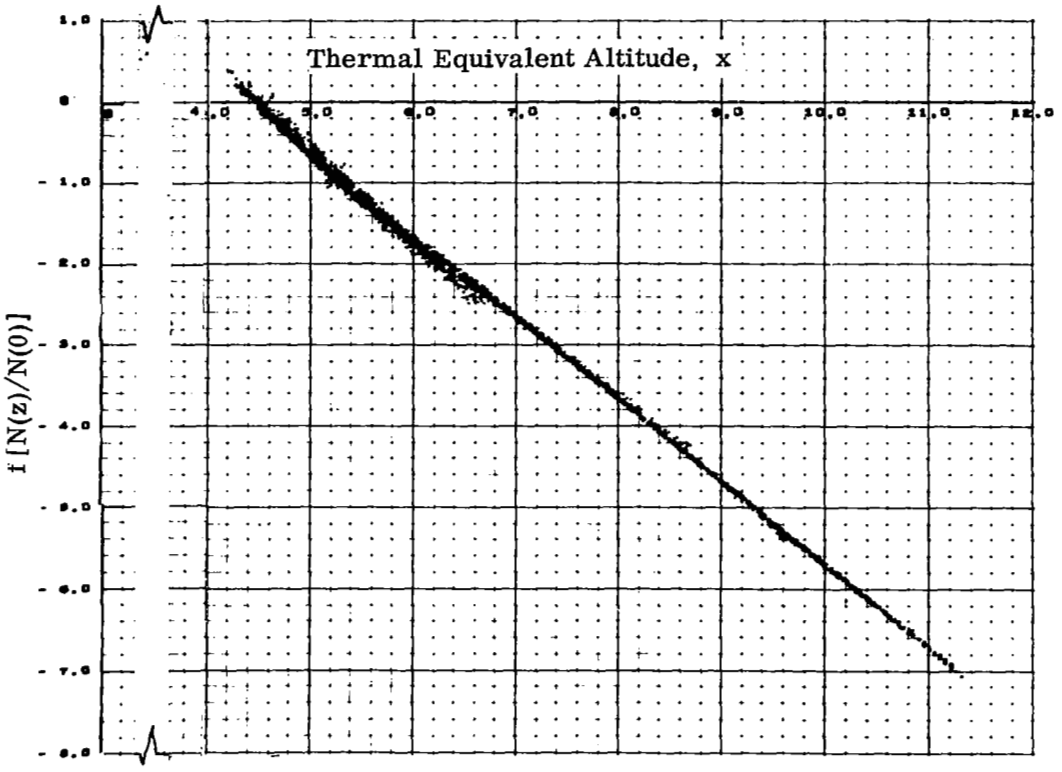

Fig. 8 Linearized Limb Radiance for Real Atmospheres

SECTION 3. – INVERSION EQUATION

3.1 Introduction

Section 2 dealt with determining the radiance by obtaining a closed form solution of the equation of radiative transfer for constant temperature gradient atmospheres. The resulting solution was written in a functional form that is linear in thermal equivalent altitude.

In this section, the linearized radiance equation is used to develop a technique for solving the inversion problem, that of inferring the atmospheric temperature from radiance measurements.

Real atmospheric temperature gradients do not, of course, extend to infinity. The assumption of Section 2 of extending to infinity was necessary only to overcome a problem in mathematics to permit a closed form solution of the equation of radiative transfer. Physically we may think of an equivalent temperature gradient or scale height gradient $\overline{\gamma\uparrow}$ above a horizon altitude which produces the same radiance as a real atmosphere. Since the weighting function determines the relative contribution to the radiance resulting from the temperature at each altitude above the horizon altitude, it is reasonable to expect that the weighting function or an approximation of it can be used to determine the relative weight of the temperature gradient at all altitudes above the horizon altitude. By definition,

$$\overline{\gamma\uparrow} \equiv \frac{\int_{s=o}^{s=\infty} \gamma \frac{\partial \tau}{\partial s}\, ds}{\int_{s=o}^{s=\infty} \frac{\partial \tau}{\partial s}\, ds} \tag{190}$$

$$\equiv \frac{1}{1 - \tau\,(s = \infty)} \int_{s=o}^{s=\infty} \gamma \frac{\partial \tau}{\partial s}\, ds \tag{191}$$

This definition permits the closed form solution of the equation of radiative transfer for constant temperature gradients developed in Section 2 to be applied to real atmospheres with variable temperature gradients.

The inversion equation is taken from the linearized radiance equation, Eq. (189)

$$G_a - x_i = \ell n - \left\{ \sqrt{\frac{T_o^2}{(T_z)_{i-1} T_a}} \left[\frac{\exp(-x_{i-1})}{(\rho_z/\rho_o)_{i-1}} \right] \frac{1}{\tau_o (T_a) K_{1/2} (\overline{\gamma_z \uparrow})_{i-1}} \right.$$

$$\left. \ell n \left[1 - \frac{N}{(1 + C'_{i-1}) B_\lambda (T°)} + B'_{i-1} \right] \right\} \qquad (192)$$

where, ignoring quadratic terms in gamma

$$B_{i-1} = \frac{C_2}{\lambda T_z} \left(\overline{\gamma_z \uparrow} \right)_{i-1} \tau_z k \frac{\sqrt{2\pi R_e H_z}}{2} \rho_z K_{3/2} \left(\overline{\gamma_z \uparrow} \right)_{i-1} \qquad (193)$$

For simplicity in the rest of this section, the mean scale height gradient $\overline{\gamma \uparrow}$ will be denoted by γ.

The value of x on the i^{th} iteration is found from the values of T_z, x, ρ_z/ρ_o, C', B', and γ on the previous iteration. The temperature is found from the value of x from

$$T = \frac{zmg}{xk}$$

The density ratio ρ_z/ρ_o at any altitude depends on the temperature variations below the altitude and a starting density ratio. The starting ratio, $e^{-x}/(\rho_z/\rho_o)$ is obtained from climatological models for the geographic location. The density ratio at each higher altitude is calculated from Eq. (112) and the density ratio at the altitude just below. Since the next subsection demonstrates convergence of the inversion method, the ability to estimate T_o and the ratio $e^{-x}/(\rho_z/\rho_o)$ on the basis of latitude and season probably represents one fundamental limitation on the accuracy of the inversion method. Percentage errors in these quantities are reduced by the thermal equivalent altitude.

3.2 Convergence

The inversion method given above is practical only if the solution converges on the correct value of temperature. The convergence requirement for the special case of an isothermal atmosphere will be developed. While an isothermal atmosphere does not exist, the analysis is easier than for a real atmosphere, and the behavior of the solution will be seen to be applicable to the general case.

For an isothermal atmosphere, the inversion equation becomes

$$x = G_a - \ell n \left[\sqrt{\frac{T}{T_a}} \frac{1}{\tau_a} \ell n \left(1 - \frac{N}{N_o} \right) \right] \tag{194}$$

The value of x on the i^{th} iteration [neglecting $K_{1/2}(\gamma)$] is given by

$$x_i = G_a - \ell n \left\{ \sqrt{\frac{T_{i-1}}{T_a}} \frac{1}{\tau_a} \ell n \left[1 - \frac{N}{\left[1 + C' \left(\frac{T_{i-1} - T}{T} \right) \right] N_o} - B'' \gamma_{i-1} \right] \right\} \tag{195}$$

where B' in Eq. (195) is equal to $B'' \gamma$. Defining ϵ_i

$$\epsilon_i = x - x_i \tag{196}$$

Substituting Eqs. (194) and (195) into the above equation and letting $\ell n (1 + x)$ be given by x

$$\epsilon_i = \ell n \left\{ \sqrt{1 + \frac{\delta_{i-1}}{T}} \frac{\left[\frac{N}{\left(1 + C' \frac{\delta_{i-1}}{T} \right) N_o} - B'' \gamma_{i-1} \right]}{N/N_o} \right\} \tag{197}$$

where δ_{i-1}, the absolute error, is defined by

$$\delta_{i-1} = T_{i-1} - T \tag{198}$$

Again, letting $\ell n (1 + x)$ be given by x

$$\epsilon_i = \frac{\delta_{i-1}}{2T} - \frac{C' \delta_{i-1}}{T} - \frac{B'' \gamma_{i-1}}{N/N_o} \tag{199}$$

But $B'' \cong \frac{C'}{2} N/N_o$. Hence

$$\epsilon_i = \frac{\delta_{i-1}}{2T} - \frac{C' \delta_{i-1}}{T} + \frac{C' \gamma_{i-1}}{2} \tag{200}$$

Now from the definition of x

$$\epsilon_i = \frac{z}{H} - \frac{z}{H_i} \tag{201}$$

or

$$\epsilon_i = \frac{\delta_i}{T} x \tag{202}$$

Equating Eqs. (200) and (202)

$$\frac{\delta_i}{\delta_{i-1}} = \frac{1}{2x} - \frac{C'}{x}\left[1 - \frac{T\,\gamma_{i-1}}{2\,\delta_{i-1}}\right] \tag{203}$$

The requirement for convergence of the inversion equation is that the absolute value of the above ratio be less than 1.0. The value of C' is very nearly that of x at altitudes near 30 km, so the ratio of $\gamma_{i-1}/\delta_{i-1}$ can become very important, demonstrating that the solution is conditionally stable.

Since for an isothermal atmosphere estimated values of γ are negligible, δ changes sign on each iteration and δ_i/δ_{i-1} may diverge. Temperature averaging (averaging T_i and T_{i-1}) is an effective means of improving convergence. Let δ_i' be the result of Eq. (203). Then for temperature averaging

$$\delta_i = \frac{\delta_i' + \delta_{i-1}}{2} \tag{204}$$

Equation (204) then becomes

$$\frac{\delta_i}{\delta_{i-1}} = \frac{1}{2}\left[1 + \frac{1}{2x} - \frac{C'}{x}\left(1 - \frac{T\,\gamma_{i-1}}{2\,\delta_{i-1}}\right)\right] \tag{205}$$

Since C'/x_{i-1} is nearly 1, in cases where γ is negligible convergence is very fast.

In practice the actual temperature is not known, so the value of δ is not known. Instead of the absolute error, use the relative error Δ_{i-1} defined by

$$\Delta_{i-1} = T_{i-1} - T_{i-2} \tag{206}$$

The convergence equation can be derived in the same way as for the absolute error yielding

$$\frac{\Delta_i}{\Delta_{i-1}} = \frac{1}{2x_{i-1}} - \frac{C'}{x_{i-1}}\left[1 - \frac{T_{i-1}\,\Gamma_{i-1}}{2\,\Delta_{i-1}}\right] \tag{207}$$

where

$$\Gamma_{i-1} = \gamma_{i-1} - \gamma_{i-2} \tag{208}$$

Similarly, for temperature averaging

$$\frac{\Delta_i}{\Delta_{i-1}} = \frac{1}{2}\left[1 + \frac{1}{2x_{i-1}} - \frac{C'}{x_{i-1}}\left(1 - \frac{T_{i-1}\,\Gamma_{i-1}}{2\,\Delta_{i-1}}\right)\right] \tag{209}$$

The criterion for convergence is that the absolute value of the above ratio be less than 1.0. However, since x, Γ, and Δ change with each new temperature estimate, convergence may only be temporary, and it is necessary to compute the relative error ratio with each iteration.

The validity of the convergence formulas in this section, for both absolute and relative errors, has been established by numerical testing.

Table 2 gives the inversion results using the general inversion equation on a 200° K isothermal atmosphere. The average absolute and relative errors decrease by nearly an order of magnitude for the first three iterations. There is little improvement in the absolute error beyond the third iteration. The slight improvement in average absolute error after the average relative error reaches a minimum makes it economically undesirable to proceed past the third iteration. Furthermore, noise prevents the absolute error from being reduced beyond a minimum value. Therefore, all inferred temperatures following are from the third iteration.

The formulas developed in Section 1 can be obtained by setting all γ's to zero in the above convergence equations. The similarity of results between table 2 for the general inversion equation and table 1 for the specialized inversion equation shows the general inversion equation is performing as expected.

TABLE 2

INVERSION RESULTS FOR A 200° K ISOTHERMAL ATMOSPHERE

Initial Estimate – 220°K

Altitude (km)	1st			2nd			3rd			4th		
	Temp (°K)	Error		Temp (°K)	Error		Temp (°K)	Error		Temp (°K)	Error	
		$T_i - T$	$T_{i-1} - T_i$		$T_i - T$	$T_{i-1} - T_i$		$T_i - T$	$T_{i-1} - T_i$		$T_i - T$	$T_{i-1} - T_i$
30	201.2	1.2	18.8	199.7	-0.1	1.5	200.2	0.2	-0.5	200.6	0.6	-0.4
32	202.1	2.1	17.8	200.2	0.2	1.9	200.3	0.3	-0.1	200.7	0.7	-0.4
34	202.7	2.7	17.3	200.4	0.4	2.3	200.4	0.4	0.0	200.7	0.7	-0.3
36	203.2	3.2	16.8	200.4	0.4	2.8	200.2	0.2	0.2	200.5	0.5	-0.3
38	203.5	3.5	16.5	200.5	0.5	3.0	200.1	0.1	0.4	200.2	0.2	-0.1
40	203.7	3.7	16.3	200.5	0.5	3.2	200.0	0.0	0.5	200.0	0.0	0.0
42	204.0	4.0	16.0	200.6	0.6	3.4	199.9	-0.1	0.7	199.9	-0.1	0.0
44	204.2	4.2	15.8	200.6	0.6	3.6	199.9	-0.1	0.7	199.8	-0.2	0.1
46	204.4	4.4	15.6	200.7	0.7	3.7	199.9	-0.1	0.8	199.8	-0.2	0.1
48	204.6	4.6	15.4	200.8	0.8	3.8	200.0	0.0	0.8	199.7	-0.3	0.3
50	204.8	4.8	15.2	201.0	1.0	3.8	200.0	0.0	1.0	199.8	-0.2	0.2
52	205.0	5.0	15.0	201.1	1.1	3.9	200.2	0.2	0.9	199.9	-0.1	0.3
54	205.2	5.2	14.8	201.3	1.3	3.9	200.3	0.3	1.0	200.0	0.0	0.3
56	205.3	5.3	14.7	201.4	1.4	3.9	200.4	0.4	1.0	200.1	0.1	0.3
58	205.4	5.4	14.6	201.5	1.5	3.9	200.4	0.4	1.1	200.1	0.1	0.3
60	205.6	5.6	14.4	201.6	1.6	4.0	200.5	0.5	1.1	200.2	0.2	0.3
Av	204.0	4.0	16.0	200.8	0.8	3.2	200.2	0.2	0.6	200.1	0.1	0.1

The situation is more complicated for real atmospheres. The K functions can no longer be ignored and the B' term can range up to 40 percent of N/N_0. However, many of the same features remain. Table 3 shows the inversion results for January 50°N atmosphere of ref. 11 with January 50°N as the first estimate of temperature.

Both the average relative and absolute errors decrease on each iteration, with relative errors decreasing by nearly an order of magnitude each time. There is little improvement beyond the third iteration. More accurate results can probably be obtained with a better starting density ratio and a better method for estimating the equivalent gamma.

TABLE 3

INVERSION RESULTS FOR JANUARY 50° N

Initial Estimate – Jan 50°N

Altitude (km)	1st			2nd			3rd			4th		
	Temp (°K)	Error		Temp (°K)	Error		Temp (°K)	Error		Temp (°K)	Error	
		$T_i - T$	$T_{i-1} - T_i$		$T_i - T$	$T_{i-1} - T_i$		$T_i - T$	$T_{i-1} - T_i$		$T_i - T$	$T_{i-1} - T_i$
30	219.4	-0.6	-0.6	219.8	-0.2	0.4	219.8	-0.2	0.0	220.0	0.0	0.3
32	222.4	-1.0	-1.0	222.5	-1.0	0.1	223.4	0.0	0.9	222.6	-0.9	-0.8
34	226.1	-1.0	-1.0	226.0	-1.1	-0.1	226.0	-1.2	0.0	225.8	-1.4	-0.2
36	229.9	-0.8	-0.8	229.8	-0.9	-0.1	229.8	-1.0	-0.1	229.8	-0.9	0.0
38	233.6	-0.6	-0.6	223.6	-0.6	0.0	233.2	-1.0	-0.4	233.1	-1.1	-0.1
40	237.6	-0.4	-0.4	237.5	-0.5	0.0	237.3	-0.7	-0.2	237.1	-0.9	-0.2
42	242.8	-0.1	-0.1	242.9	0.0	0.1	242.8	-0.1	0.0	242.4	-0.5	-0.4
44	248.3	0.3	0.3	248.7	0.6	0.3	248.8	0.8	0.1	248.8	0.8	0.0
46	252.3	0.5	0.5	252.7	1.0	0.4	252.9	1.2	0.2	253.0	1.2	0.1
48	255.8	1.0	1.0	256.5	1.6	0.7	256.9	2.1	0.4	257.3	2.4	0.3
50	256.4	1.4	1.4	257.3	2.3	0.9	258.0	3.0	0.7	258.6	3.6	0.6
52	251.0	1.3	1.3	251.8	2.1	0.8	252.5	2.8	0.6	253.0	3.3	0.6
54	243.0	1.0	1.0	243.7	1.7	0.7	244.2	2.2	0.5	244.6	2.6	0.4
56	237.6	0.9	0.9	238.2	1.5	0.6	238.6	1.9	0.4	239.0	2.2	0.4
58	233.7	0.7	0.7	234.2	1.2	0.5	234.5	1.5	0.3	234.8	1.8	0.3
60	231.5	0.5	0.5	231.9	0.9	0.4	232.1	1.1	0.2	232.3	1.3	0.2
Av	-	0.2	0.2	-	0.5	0.4	-	0.8	0.2	-	0.8	0.1

An attempt was made to increase stability by changing γ in the proper direction as indicated by Eq. (209) whenever the relative error increased. This kept the relative error from diverging. However, in some cases, the minimum relative error thus obtained is quite large. More effort is required to assure satisfactory stability of the solution.

3.3 Inversion Results

The temperatures obtained from the inversion program for a climatological model atmosphere are given in fig. 9. The real atmosphere is the January 50° N atmosphere from ref. 9. The inferred temperatures are those of the third iteration in table 3. The absorption coefficients are based on fig. 7. In Appendix C, tables 10 through 13 give the results for various climatological conditions.

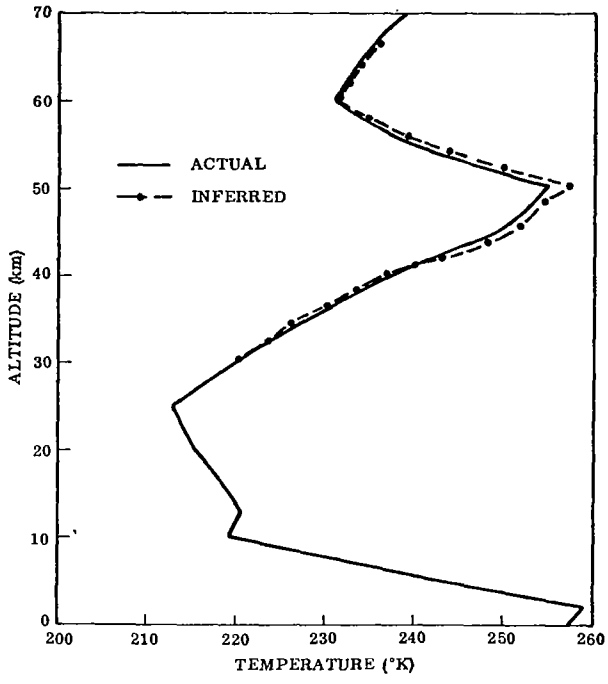

Fig. 9 Comparison of Actual and Inferred Temperature Profiles for January 50° N

There is a problem near the stratopause at 50 km, probably due to errors in estimating the equivalent gamma. It is the inferred temperatures at altitudes around 50 km that cause the average absolute error to be as large as it is.

A crucial test of the inversion program is its ability to perform properly in the presence of noise and bias errors. Table 4 shows the inferred temperatures and absolute errors on the third pass for the case of no radiance error and three cases of different radiance errors.

The effect of a +5-percent increase in the radiance at each altitude was to increase the average temperature error by approximately one degree. The change of temperature decreases with increasing x, being 1.9° K at 30 km and decreasing to 0.5° K at 60 km.

TABLE 4

INVERSION RESULTS FOR JANUARY 50° N WITH AND WITHOUT RADIANCE ERROR

Initial Estimate – Jan 40°N

Altitude (km)	Actual Temp (°K)	No Error		+5% Radiance Error		Bias Error (100% at 60 km)		Bias and Noise Error	
		Temp (°K)	Error (°K)	Temp (°K)	Error (°K)	Temp (°K)	Error (°K)	Temp (°K)	Error (°K)
30	220.0	221.2	1.2	223.1	3.1	221.9	1.9	220.4	0.4
32	223.6	223.9	0.3	225.5	1.9	224.7	1.1	223.3	-0.3
34	227.2	227.6	0.4	229.1	1.9	228.6	1.4	227.8	0.6
36	230.8	231.5	0.7	232.8	2.0	232.6	1.8	231.5	0.7
38	234.4	235.0	0.6	236.3	1.9	236.4	2.0	233.4	-1.0
40	238.0	239.6	1.6	240.8	2.8	241.2	3.2	236.6	-1.4
42	242.8	242.8	0.0	244.0	1.2	244.9	2.1	241.8	-1.0
44	247.6	247.5	-0.1	248.5	0.9	250.0	2.4	247.7	0.1
46	251.0	249.4	-1.6	250.4	-0.6	252.7	1.7	249.8	-1.2
48	253.0	251.1	-1.9	252.0	-1.0	255.5	2.5	251.4	-1.6
50	255.0	258.8	3.8	259.5	4.5	263.7	8.7	258.9	3.9
52	248.6	251.8	3.2	252.5	3.9	256.5	7.9	251.5	2.9
54	242.2	244.1	1.9	244.8	2.6	252.6	10.4	244.0	1.8
56	237.4	238.5	1.1	239.1	1.7	249.7	12.3	238.2	0.8
58	234.2	234.7	0.5	235.8	1.6	248.7	14.5	235.1	0.9
60	231.0	230.9	-0.1	231.4	0.4	245.1	14.1	230.9	-0.1
Av	–	–	0.7	–	1.8	–	–	–	0.4

The next two columns give the error due to a constant error in radiance, which is 100 percent at 60 km. The change in temperature increases rapidly with altitude, so no average of the absolute error is taken.

Figure 10 shows the relative error in temperature as a function of the bias error, as a percent of the radiance at the given altitude. The relative error is the difference between the inferred temperature with no error and the inferred temperature with the bias error. The rather large temperature errors in table 4 are seen from fig. 10 to be due to very large bias errors.

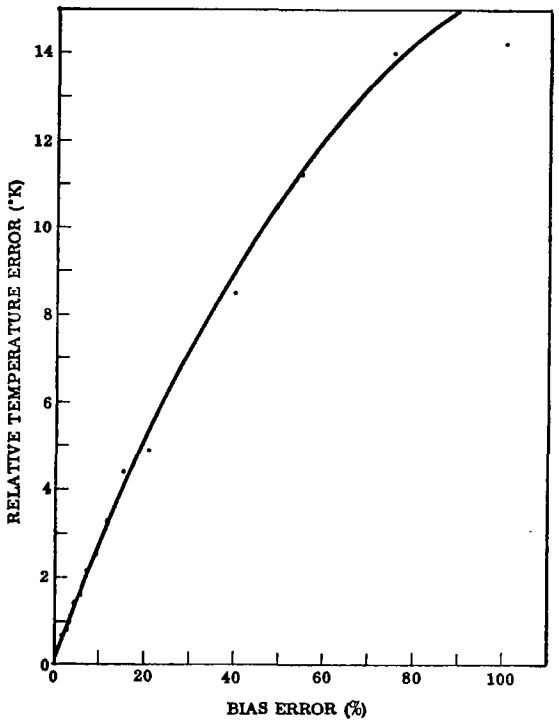

Fig. 10 Relative Temperature Error Resulting From a Bias Radiance

The last two columns give the error due to a combined bias and noise error in radiance. The radiance data used for the no-error case has four significant figures. The radiance for the noise-and-bias case was obtained by truncating the radiance values to two significant figures. The noise in this case is not random since large values of radiance noise are not permitted. The average radiance error is -1.5 percent. Scaling this according to the results for the +5-percent radiance error, the average absolute error should be decreased by 0.3 degree. This prediction is correct, as is seen from the table. The effect of noise, which ranges up to 5 percent, is seen to be of small importance at individual altitude points and does not change the average error.

SECTION 4. – ANALYSIS OF PROJECT SCANNER FLIGHT DATA

The results of the two Project Scanner flights (refs. 12 and 13) offer an opportunity to test the inversion technique developed in Sections 1 and 2 with real world data. Both flights were suborbital launches from Wallops Island, Virginia; the first was launched on August 16, 1966, and the second on December 10, 1966. The data used in the following analysis (presented in Appendix D for convenient reference) are taken from refs. 12 and 13.

Model atmospheres were derived for geographical areas (cells) where atmospheric conditions were relatively uniform, and the measured radiance profiles were averaged for each cell. This provides the opportunity to compute the mean absorption coefficient for real atmospheres, as was done in Section 1 for isothermal atmospheres. The mean absorption coefficient was calculated for every 2 km from 30 to 60 km for each cell of the summer experiment. These results are presented in table 5 and fig. 11. It is clear that above 50 km, where the radiometer signal-to-noise ratio is low and the error in measured temperature is high, there is considerable spread in the data. The coefficients for Cells 1, 2, 3, and 7 are in substantial agreement as are the coefficients for Cells 4 and 6. Except for Cell 5 above 50 km, all the cells have the same characteristics with altitude.

It is the trend with altitude that is of particular significance. Rather than tending toward a constant value when the atmosphere is optically thin as anticipated and as occurred for the analytical profiles for isothermal atmospheres, the mean absorption coefficients increase with altitude. This implies that the absorption at high altitudes (low pressure) is greater than anticipated from the Elsasser model for carbon dioxide transmissivity. Greater absorption would mean higher values of radiance.

The coefficients for Cells 1, 2, 3, and 7 were averaged at each geometric altitude. Ideally, the averaging should be done at the same values of thermal equivalent altitude; but, with the errors in the data, this would be an undue complication. The results, plotted in fig. 12, show an almost linear increase with altitude except at low altitudes where an upward bowing occurs similar to the isothermal curves.

Shown also are the high and low limits of the coefficient at each altitude. As expected, the spread in the data increases with decreasing signal-to-noise ratios and increasing error in temperature measurement. The average values were used to infer temperature from individual radiance profiles taken from Cells 1, 2, 3, and 7.

The mean absorption coefficients were calculated for the winter Cell 1 (ref. 13). The model atmosphere for Trout Lake (53°50'N, 89°52'W) was assumed to correspond to Cell 1 at 57°N, 92°W. Figure 13 presents the results and includes, for comparison, the average data from fig. 12. The general trend of the curve is the same; however, the curve is displaced upward an appreciable amount. Except for possible temperature and density curve correction, it is desirable that the mean absorption curve be independent of geographic location, season, and other parameters. Within experimental error, the data of fig. 11 indicate that this may be the case.

TABLE 5

MEAN ABSORPTION COEFFICIENTS FOR PROJECT SCANNER SUMMER DATA

$k \times 10^6$

Altitude (km)	Cell 1		Cell 2		Cell 3		Cell 4		Cell 5		Cell 6		Cell 7	
	x	k	x	k	x	k	x	k	x	k	x	k	x	k
30	4.32	377	4.32	387	4.28	374	4.36	339	4.41	320	4.47	365	4.51	393
32	4.55	397	4.57	406	4.57	396	4.55	366	4.53	337	4.60	365	4.64	385
34	4.78	408	4.79	421	4.79	414	4.77	383	4.71	357	4.75	385	4.77	401
36	4.95	412	4.98	426	4.96	426	4.94	402	4.90	381	4.92	406	4.92	429
38	5.07	426	5.11	447	5.11	442	5.13	407	5.11	400	5.13	419	5.13	452
40	5.19	460	5.23	482	5.25	468	5.27	431	5.31	408	5.33	421	5.33	448
42	5.39	511	5.42	500	5.45	486	5.45	456	5.47	418	5.47	426	5.47	479
44	5.78	497	5.62	519	5.64	606	5.64	474	5.62	439	5.57	445	5.70	485
46	5.80	536	5.84	548	5.84	533	5.84	491	5.84	454	5.78	476	5.74	531
48	6.07	564	6.12	570	6.10	582	6.12	512	6.12	467	6.10	501	6.00	554
50	6.34	581	6.39	596	6.42	620	6.42	522	6.42	462	6.42	491	6.42	559
52	6.69	596	6.75	603	6.72	656	6.70	528	6.60	455	6.55	486	6.52	563
54	7.01	602	7.08	642	7.06	689	6.98	535	6.77	444	6.64	528	6.64	580
56	7.30	616	7.38	667	7.37	669	7.31	532	7.12	421	7.04	524	7.06	528
58	7.59	664	7.68	644	7.69	732	7.66	581	7.48	414	7.46	558	7.49	540
60	7.89	673	7.98	661	8.01	859	8.01	733	7.86	457	7.89	644	7.95	626

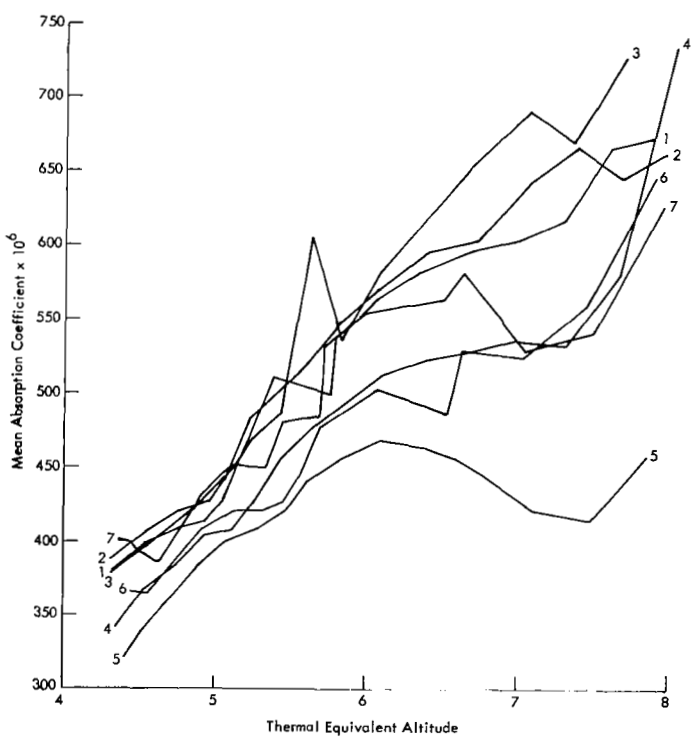

Fig. 11 Computed Mean Absorption Coefficient for Project Scanner Summer Data

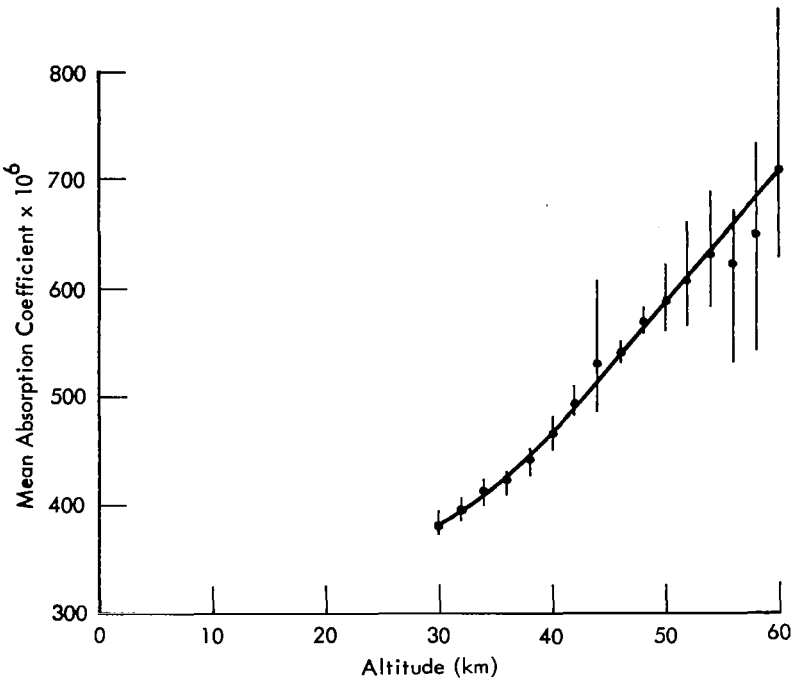

Fig. 12 Average, High, and Low Mean Absorption Coefficients for Cells 1, 2, 3, and 7

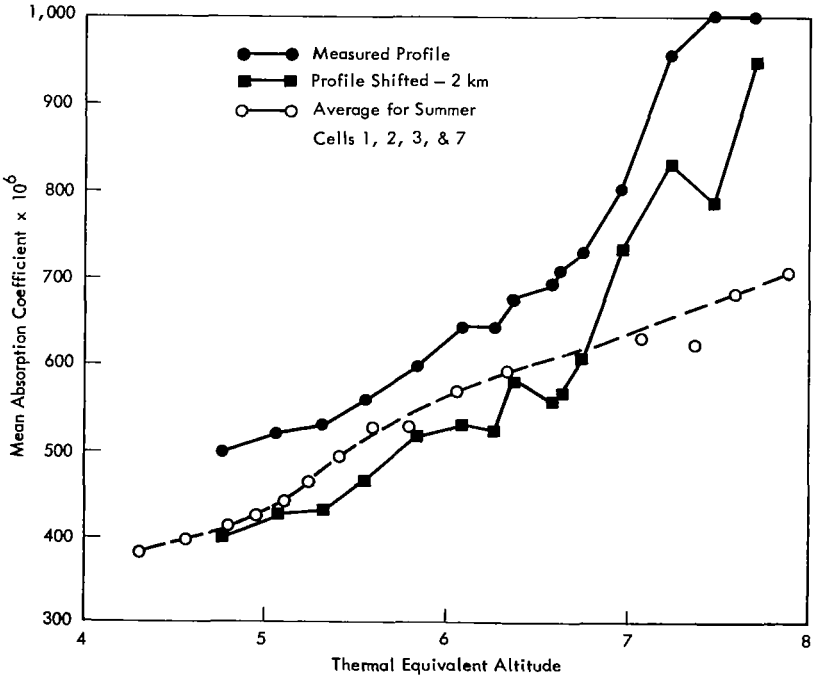

Fig. 13 Mean Absorption Coefficients for Winter Cell 1

Before any conclusions can be drawn, it is necessary to determine if the differences between the various mean absorption coefficient curves is within the experimental error. The difficulty in making conclusions about these particular data due to strong horizontal fields is pointed out in ref. 13. However, since these data are obtained on a different flight, a possible bias error exists between the two flights. To test the sensitivity of the coefficients to tangent height accuracy, the radiance profile was arbitrarily shifted down by 2 km. The value of x did not change since it was calculated from the Trout Lake atmosphere. As a result, the calculated mean absorption curve (fig. 13) is below the average curve for summer Cells 1, 2, 3, and 7.

A downward shift of approximately 1.6 km would have provided a good fit. This does not suggest a probable bias error in tangent height of 1.6 km as other sources of error, such as any possible temperature correction, must be considered. However, 1.6 km is within the joint distribution of tangent height error. Therefore, it is not possible to say if the difference in absolute value of the mean absorption coefficients is significant.

Using the average absorption coefficients for Cells 1, 2, 3, and 7, the average radiance profiles for each cell were used to infer the model atmosphere for each cell, respectively. By using the answer as the starting estimate, a good test of accuracy, convergence, and stability is provided in the presence of noise. For each case, the results of the first three passes through the inversion program are given in tables 6, 7, 8, and 9. The program has converged on the correct temperatures after no more than one iteration in all cases. The results for Cell 3 (table 8) demonstrate the conditional stability of the solution. Here, the average absolute error is slowly increasing although the relative error does not change appreciably. Even so, the results up to 50 km (with the singular exception of 44 km) demonstrate stability; difficulty above 50 km is to be expected because of the low signal-to-noise ratio and possible high MRN temperature measurement errors. The same difficulty is not experienced for Cell 7, as the differences between the small values of the absolute and relative errors are not significant.

A measured radiance profile from each cell was selected. They were selected so as not to have four similar radiance profiles. The temperature difference between the inferred temperature profile and the model temperature profile for the particular cell is given for each cell in table 10. Also given at the bottom is the number of passes through the inversion program to obtain convergence. A weighting factor was applied permitting larger relative errors at high altitudes. Without the weighting factors, Cell 3 requires one iteration to indicate convergence. With the singular exception of 38 km in Cell 1, all of the differences are within MRN temperature accuracy (ref. 13). The difference of -2.4°K at 30 km in Cell 1 can exist with the strong temperature fields at high latitudes during the summer. In no case was there a stability problem.

In summary, this analysis of Project Scanner data demonstrates that the inversion program is convergent with noisy data and yields temperature profiles that are accurate within the limits of present MRN data. An attempt should be made to explain the apparent increase of mean absorption coefficient with altitude.

TABLE 6

INVERSION RESULTS FOR CELL 1 AVERAGE DATA (SUMMER)

Altitude (km)	1st			2nd			3rd		
	Temperature (°K)	Error		Temperature (°K)	Error		Temperature (°K)	Error	
		$T_i - T$	$T_{i-1} - T_i$		$T_i - T$	$T_{i-1} - T_i$		$T_i - T$	$T_{i-1} - T_i$
30	233.5	-1.4	-1.4	234.3	-0.7	0.7	234.0	-1.0	-0.3
32	236.7	-1.1	-1.1	237.7	-0.5	0.6	237.3	-0.5	0.0
34	239.2	-1.4	-1.4	239.6	-1.0	0.5	239.7	-0.9	0.1
36	243.6	-2.0	-2.0	243.6	-2.0	0.0	243.6	-2.0	0.0
38	250.9	-1.9	-1.9	250.6	-2.2	-0.3	250.4	-2.4	-0.2
40	259.3	-0.7	-0.7	259.4	-0.6	0.1	259.5	-0.5	0.1
42	263.5	0.7	0.7	264.2	1.4	0.7	265.1	2.3	0.9
44	254.4	-2.2	-2.2	253.6	-3.0	-0.8	252.8	-3.8	-0.8
46	266.9	-0.1	-0.1	266.8	-0.2	-0.1	266.9	-0.1	0.1
48	266.0	0.0	0.0	265.9	-0.1	-0.1	265.8	-0.2	-0.1
50	265.1	0.1	0.1	265.0	0.0	-0.1	265.1	0.1	0.1
52	261.4	0.0	0.0	261.4	0.0	0.0	261.4	0.0	0.0
54	258.4	-0.4	-0.4	258.5	-0.3	0.1	258.5	-0.3	0.0
56	257.8	0.3	0.3	258.0	0.5	0.2	258.3	0.8	0.3
58	257.0	0.7	0.7	257.7	1.4	0.7	258.4	2.0	0.6
60	254.1	-0.9	-0.9	253.8	-1.2	-0.3	253.5	-1.5	-0.3
Average	—	-0.6	-0.6	—	-0.6	0.1	—	-0.6	<0.1

TABLE 7

INVERSION RESULTS FOR CELL 2 AVERAGE DATA (SUMMER)

Altitude (km)	1st			2nd			3rd		
	Temperature (°K)	Error		Temperature (°K)	Error		Temperature (°K)	Error	
		$T_i - T$	$T_{i-1} - T_i$		$T_i - T$	$T_{i-1} - T_i$		$T_i - T$	$T_{i-1} - T_i$
30	234.3	-0.7	-0.7	234.6	-0.4	0.3	234.5	-0.5	-0.1
32	236.5	-0.5	-0.5	236.8	-0.2	0.3	236.8	-0.2	0.0
34	239.4	-0.6	-0.6	239.7	-0.3	0.3	239.8	-0.2	0.1
36	243.0	-1.0	-1.0	242.8	-1.2	-0.2	241.1	-2.9	-1.7
38	250.3	-0.7	-0.7	250.1	-0.9	-0.2	250.2	-0.8	0.1
40	258.3	0.3	0.3	258.7	0.7	0.4	259.0	1.0	0.3
42	260.8	-0.2	-0.2	261.0	0.0	0.2	261.0	0.0	0.0
44	263.3	-0.7	-0.7	263.1	-0.9	-0.2	262.7	-1.3	-0.4
46	265.4	0.4	0.4	265.8	0.8	0.4	266.1	1.1	0.3
48	264.2	0.2	0.2	264.4	0.4	0.2	264.6	0.6	0.2
50	263.5	0.5	0.5	264.0	1.0	0.5	264.3	1.3	0.3
52	259.2	0.2	0.2	259.4	0.4	0.2	259.5	0.5	0.1
54	256.6	0.6	0.6	257.1	1.1	0.5	257.3	1.3	0.2
56	256.3	1.6	1.6	257.4	2.7	1.1	258.3	3.6	0.9
58	253.8	0.5	0.5	254.2	0.9	0.4	254.6	1.3	0.4
60	251.3	-0.7	-0.7	250.9	-1.1	-0.4	250.5	-1.5	-0.4
Average	—	<0.1	<0.1	—	0.2	0.2	—	0.2	<0.1

TABLE 8

INVERSION RESULTS FOR CELL 3 AVERAGE DATA (SUMMER)

Altitude (km)	1st			2nd			3rd		
	Temperature (°K)	Error		Temperature (°K)	Error		Temperature (°K)	Error	
		$T_i - T$	$T_{i-1} - T_i$		$T_i - T$	$T_{i-1} - T_i$		$T_i - T$	$T_{i-1} - T_i$
30	235.3	-1.7	-1.7	235.8	-1.2	0.5	235.4	-1.6	-0.4
32	235.8	-1.2	-1.2	236.3	-0.7	0.5	236.2	-0.8	-0.1
34	238.9	-1.1	-1.1	239.2	-0.8	0.3	239.1	-0.9	-0.1
36	244.0	-1.0	-1.0	244.3	-0.7	0.3	244.3	-0.7	0.0
38	249.9	-1.1	-1.1	250.0	-1.1	0.0	250.6	-0.4	0.7
40	256.5	-0.5	-0.5	256.8	-0.2	0.3	256.8	-0.2	0.0
42	259.1	-0.9	-0.9	258.7	-1.3	-0.4	258.2	-1.8	-0.5
44	266.0	3.0	3.0	268.3	5.3	2.2	270.2	7.2	1.9
46	264.8	-0.2	-0.2	265.0	0.0	0.2	264.8	-0.2	-0.2
48	265.6	0.6	-0.6	266.2	1.2	0.6	266.5	1.5	0.3
50	263.1	1.1	1.1	263.9	1.9	0.8	264.4	2.4	0.5
52	261.7	1.7	1.7	262.9	2.9	1.2	263.8	3.8	0.9
54	258.8	1.8	1.8	260.2	3.2	1.3	261.2	4.2	1.0
56	256.6	1.6	1.6	257.7	2.7	1.1	258.5	3.5	0.8
58	255.1	2.1	2.1	256.6	3.6	1.5	257.8	4.8	1.2
60	253.3	2.3	2.3	255.0	4.0	1.7	256.4	5.4	1.4
Average	—	0.6	0.6	—	1.2	0.8	—	1.6	0.5

TABLE 9

INVERSION RESULTS FOR CELL 7 AVERAGE DATA (SUMMER)

Altitude (km)	1st			2nd			3rd		
	Temperature (°K)	Error		Temperature (°K)	Error		Temperature (°K)	Error	
		$T_i - T$	$T_{i-1} - T_i$		$T_i - T$	$T_{i-1} - T_i$		$T_i - T$	$T_{i-1} - T_i$
30	225.5	0.5	0.5	225.9	0.9	0.4	225.8	0.8	-0.1
32	231.8	-1.2	-1.2	231.3	-1.7	-0.5	231.1	-1.9	-0.2
34	240.2	-0.8	-0.8	239.5	-1.5	-0.7	238.9	-2.1	-0.6
36	247.7	0.7	0.7	247.8	0.8	0.1	247.7	0.7	-0.1
38	251.0	1.0	1.0	251.4	1.4	0.4	251.9	1.9	0.5
40	252.5	-0.5	-0.5	252.0	-1.0	-0.5	251.6	-1.4	-0.4
42	258.9	-0.1	-0.1	258.9	-0.1	0.0	258.8	-0.2	-0.1
44	258.5	-1.5	-1.5	257.2	-2.8	-1.3	255.9	-4.1	-1.3
46	271.1	1.1	1.1	271.6	1.6	0.5	271.8	1.8	0.2
48	270.1	1.1	1.1	270.6	1.6	0.5	271.1	2.1	0.5
50	261.9	-0.1	-0.1	261.9	-0.1	0.0	261.8	-0.2	-0.1
52	268.0	0.0	0.0	267.9	-0.1	-0.1	267.7	-0.3	-0.2
54	273.4	0.4	0.4	273.7	0.7	0.3	273.9	0.9	0.2
56	265.5	-0.8	-0.8	265.0	-1.3	-0.5	264.4	-1.9	-0.6
58	258.8	-0.9	-0.9	258.1	-1.6	-0.7	257.5	-2.2	-0.6
60	252.7	-0.3	-0.3	252.4	-0.6	-0.3	252.2	-0.8	-0.2
Average	—	-0.1	-0.1	—	-0.2	-0.2	—	-0.4	-0.2

TABLE 10

INVERSION PROJECT RESULTS FOR MEASURED RADIANCE PROFILES FROM THE SUMMER SCANNER FLIGHT

Altitude (km)	Latitude/Longitude			
	56.2°/66.5°	52.2°/54.1°	46.3°/48.7°	13.8°/56.3°
	Cell 1	Cell 2	Cell 3	Cell 7
30	-2.4	-0.7	-0.4	1.3
32	-1.7	-0.7	0.4	-1.5
34	-2.1	-1.1	0.3	-0.5
36	-2.0	-1.9	0.3	0.4
38	-5.4	-2.0	0.4	1.5
40	-1.8	-1.4	0.9	0.2
42	0.7	-2.2	0.7	3.1
44	-4.4	-3.2	0.4	0.7
46	-0.9	-1.8	1.2	4.8
48	-1.9	0.0	1.5	4.1
50	-1.9	1.1	1.8	2.9
52	-0.7	-0.4	2.7	4.4
54	0.0	0.2	3.6	4.3
56	2.0	2.9	4.5	3.4
58	2.2	1.7	5.2	4.5
60	-0.9	-0.9	5.2	0.3
No. of Passes	3	2	1	2

APPENDIX A
PLANETARY THERMAL CONSTANT

It has been shown by King (ref. 5) that the transmission for a gray atmosphere is given by

$$\tau = \exp - \left[e^{-(z-\eta)/H} \right] \tag{A1}$$

where

$$\eta = H \ell n \left[\sqrt{\frac{2\pi R_e}{H}} (k \rho_o H) \right] \tag{A2}$$

Equation (A2) can be written in a form that reveals the physical significance of the factors as follows:

$$\eta = H \left[G + \ell n \tau_o \right] \tag{A3}$$

where

$$G = \frac{1}{2} \ell n \left(\frac{2\pi R_e}{H} \right) \tag{A4}$$

and

$$\tau_o = k \rho_o H \tag{A5}$$

The optical thickness of the atmosphere τ_o is unitless and is a combination of important parameters of the atmosphere.

King pointed out the significance of the planetary thermal constant G. The scale height H is given by

$$H = \frac{kT}{mg} \tag{A6}$$

Substituting for H in Eq. (A4)

$$G = \frac{1}{2} \ell n \left(\frac{2\pi R_e mg}{kT} \right) \tag{A7}$$

The acceleration of gravity g near the earth's surface is given by

$$g = \frac{G_o M_e}{R_e^2} \tag{A8}$$

where

G_o = gravitational constant
M_e = mass of the earth

Substituting for g in Eq. (A7)

$$G = \frac{1}{2} \ell n \left[\frac{\pi \left(\frac{G_o M_e m}{R_e} \right)}{1/2\ kT} \right] \tag{A9}$$

The gravitational potential energy of a molecule of mass m is the expression in the parentheses. The kinetic energy per degree of freedom for a particle of mass m is 1/2 kT. Hence G can be written

$$G = \frac{1}{2} \ell n \left(\pi \frac{G.\ P.\ E.}{K.\ E.} \right) \tag{A10}$$

where

G. P. E. = gravitational potential energy
K. E. = kinetic energy

APPENDIX B
K FUNCTIONS

The K functions are the functions $K_{n/2}(\gamma)$ in Section 2. They enable integrals over transmission, for an atmosphere with a linear temperature gradient, to be simply expressed in terms of a corresponding integral for an isothermal atmosphere.

From Section 1, the value of u_∞ for an isothermal atmosphere can be expressed as

$$u_\infty = \sqrt{2\pi R_e H}\ \rho_z \tag{B1}$$

where

$$\rho_z = \rho_o\, e^{-z/H} \tag{B2}$$

For an isothermal atmosphere H is a constant with altitude.

From subsection 2.1, the value of u_∞ for an atmosphere with a positive scale height gradient γ is given by

$$u_\infty = \sqrt{2\pi R_e H_z}\,\frac{\rho_z}{\sqrt{\gamma}}\,\frac{\Gamma(1/\gamma + 1/2)}{\Gamma(1/\gamma + 1)} \tag{B3}$$

Defining $K_{1/2}(\gamma)$

$$K_{1/2}(\gamma) = \frac{1}{\sqrt{\gamma}}\,\frac{\Gamma(1/\gamma + 1/2)}{\Gamma(1/\gamma + 1)} \tag{B4}$$

The expression for u_∞ becomes

$$u_\infty = \sqrt{2\pi R_e H_z}\,\rho_z\, K_{1/2}(\gamma) \tag{B5}$$

It is seen that u_∞ is equivalent to the expression for an isothermal atmosphere, with H equal to H_z, times the factor $K_{1/2}(\gamma)$. The function $K_{1/2}(\gamma)$ expresses the change in u_∞ due to the temperature gradient above the horizon altitude z.

The function $K_{1/2}(\gamma)$ can be numerically evaluated easily using Stirling's formula. Stirling's formula is accurate for even small values of x and states that

$$\Gamma(x) = e^{-x}\, x^x \sqrt{\frac{2\pi}{x}} \tag{B6}$$

Using this approximation, $K_{1/2}(\gamma)$ is given by

$$K_{1/2}(\gamma) = \left(\frac{e}{1+\gamma}\right)^{1/2} \left(\frac{1+\gamma/2}{1+\gamma}\right)^{1/\gamma} \tag{B7}$$

In the limit as γ approaches zero, $K_{1/2}(\gamma)$ approaches one.

From subsection 2.2, the value of u_∞ for an atmosphere with a negative scale height gradient is given by

$$u_\infty = \sqrt{2\pi R_e H_z}\, \frac{\rho_z}{\sqrt{(-\gamma)}}\, \frac{\Gamma\left(1/(-\gamma)\right)}{\Gamma\left(1/(-\gamma)+1/2\right)} \tag{B8}$$

In this case, $-\gamma$ is a positive quantity. The function $K_{1/2}(-\gamma)$ is then defined by

$$K_{1/2}(-\gamma) = \frac{1}{\sqrt{(-\gamma)}}\, \frac{\Gamma\left(1/(-\gamma)\right)}{\Gamma\left(1/(-\gamma)+1/2\right)} \tag{B9}$$

Using Stirling's formula

$$K_{1/2}(-\gamma) = e^{1/2}\left(\frac{1}{1+(-\gamma)/2}\right)^{1/(-\gamma)} \tag{B10}$$

The other integrals in Section 2 were evaluated in terms of the gamma function. Using Stirling's formula, the general formula for the K functions for positive γ becomes

$$K_{n/2}(\gamma) = \left(\frac{e}{1+\gamma}\right)^{n/2} \left[1 - \frac{n\gamma}{2(1+\gamma)}\right]^{\frac{1}{\gamma}-\frac{n-1}{2}}$$

Similarly for negative γ, the general function becomes

$$K_{n/2}(-\gamma) = e^{n/2}\left[\frac{1}{1+\frac{n(-\gamma)}{2}}\right]^{\frac{1}{(-\gamma)}+\frac{n-1}{2}}$$

In both cases, n is limited to odd integers. Figure 14 is a plot of the K functions for n = 1, 3, and 5. The K functions are plotted as a function of the temperature gradient rather than γ.

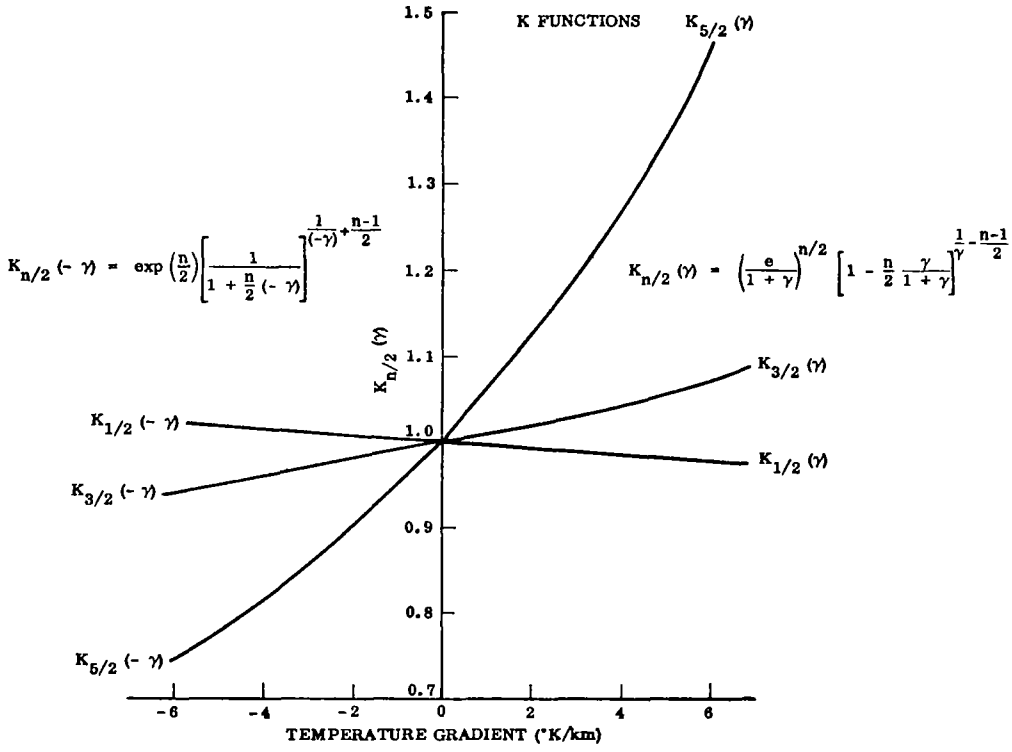

Fig. 14 K Functions

APPENDIX C

VARIOUS CLIMATOLOGICAL RESULTS

Inversion results for climatological models (ref. 9) representing arctic winter, arctic summer, temperate summer, and equatorial regions are presented in this appendix. The arctic winter is represented by January 90° N with January 80° N for the initial estimate. The solution has converged on the second pass or first iteration. Arctic summer is represented by July 90° N with July 80° N for the initial estimate. Again, the solution has converged on the first iteration. Temperate summer is represented by August 40° N with August 50° N for the initial estimate. The equatorial region is represented by January 0° with January 10° N for the initial estimate. For both of these cases, the solution has converged on the first pass. This result is to be expected in equatorial regions where the temperature fields have small spatial variation.

TABLE 11

INVERSION RESULTS FOR ARCTIC WINTER (JAN 90° N)

Initial Estimate – Jan 80° N

Altitude (km)	1st			2nd			3rd		
	Temp. (°K)	Error		Temp. (°K)	Error		Temp (°K)	Error	
		$T_i - T$	$T_{i-1} - T_i$		$T_i - T$	$T_{i-1} - T_i$		$T_i - T$	$T_{i-1} - T_i$
30	198.1	- 1.9	2.9	199.2	- 0.8	- 1.1	199.0	- 1.0	0.2
32	199.7	- 2.8	3.2	200.3	- 2.2	- 0.6	200.1	- 2.4	0.2
34	204.3	- 3.2	3.3	204.6	- 3.0	- 0.3	204.8	- 2.8	- 0.2
36	208.9	- 3.3	3.3	209.0	- 3.3	- 0.1	209.0	- 3.3	0.0
38	213.8	- 3.1	3.0	213.9	- 3.1	- 0.1	213.8	- 3.1	0.1
40	219.3	- 2.7	2.7	219.4	- 2.6	- 0.1	219.4	- 2.6	0.0
42	225.3	- 1.8	2.4	225.5	- 1.7	- 0.2	225.4	- 1.8	0.1
44	231.8	- 1.0	2.0	232.0	- 0.8	- 0.2	232.0	- 0.8	0.0
46	239.1	- 1.1	1.7	239.4	- 0.8	- 0.3	239.5	- 0.8	- 0.1
48	249.0	- 1.6	0.7	249.6	- 1.0	- 0.6	250.2	- 0.4	- 0.6
50	253.9	- 2.1	0.1	253.8	- 2.2	0.1	253.8	- 2.2	0.0
52	248.5	- 2.0	0.1	248.4	- 2.1	0.1	248.2	- 2.3	0.2
54	238.7	- 1.5	0.1	238.7	- 1.5	0.0	238.8	- 1.4	- 0.1
56	231.8	- 0.8	0.1	232.2	- 0.4	- 0.4	232.8	0.2	- 0.6
58	226.4	0.1	0.2	226.7	0.4	- 0.3	227.3	1.0	- 0.6
60	223.8	0.8	0.2	223.8	0.8	0.0	224.0	1.0	- 0.2
Avg.	–	- 1.7	1.6	–	- 1.5	- 0.3	–	- 1.4	- 0.1

TABLE 12

INVERSION RESULTS FOR ARCTIC SUMMER (JUL 90° N)

Initial Estimate – Jul 80° N

Altitude (km)	1st			2nd			3rd		
	Temp. (°K)	Error		Temp. (°K)	Error		Temp. (°K)	Error	
		$T_i - T$	$T_{i-1} - T_i$		$T_i - T$	$T_{i-1} - T_i$		$T_i - T$	$T_{i-1} - T_i$
30	249.0	5.0	- 6.0	246.0	2.0	3.0	248.0	4.0	- 2.0
32	252.8	2.9	- 3.8	250.6	0.6	2.2	251.1	1.1	- 0.5
34	259.2	2.4	- 3.3	257.2	0.4	2.0	257.2	0.4	- 0.0
36	265.3	2.3	- 3.3	263.6	0.6	1.7	263.5	0.6	0.1
38	271.2	2.6	- 3.6	269.8	1.2	1.4	269.8	1.1	0.0
40	276.7	2.7	- 3.7	275.6	1.6	1.1	275.6	1.6	0.0
42	282.0	2.8	- 3.8	281.1	1.9	0.9	281.1	1.9	0.0
44	286.9	3.0	- 4.0	286.2	2.3	0.7	286.4	2.4	- 0.2
46	291.2	3.4	- 4.2	290.7	2.9	0.5	290.9	3.1	- 0.2
48	295.0	4.2	- 4.5	294.9	4.1	0.1	295.0	4.2	- 0.1
50	297.8	4.8	- 4.8	298.0	5.0	- 0.2	298.5	5.5	- 0.5
52	299.0	4.3	- 4.9	299.6	4.9	- 0.6	300.2	5.6	- 0.6
54	298.8	3.4	- 5.0	299.8	4.4	- 1.0	300.7	5.3	- 0.9
56	296.6	2.4	- 4.8	297.7	3.5	- 1.1	298.8	4.6	- 1.1
58	292.9	1.4	- 4.6	294.2	2.6	- 1.2	295.4	3.8	- 1.2
60	286.1	0.1	- 4.1	287.2	1.2	- 1.1	288.4	2.4	- 1.2
Avg.	–	3.0	- 4.3	–	2.5	0.5	–	3.0	- 0.5

TABLE 13

INVERSION RESULTS FOR TEMPERATE SUMMER (AUG 40° N)

Initial Estimate – Aug 50° N

Altitude (km)	1st			2nd			3rd		
	Temp. (°K)	Error		Temp. (°K)	Error		Temp. (°K)	Error	
		$T_i - T$	$T_{i-1} - T$		$T_i - T$	$T_{i-1} - T_i$		$T_i - T$	$T_{i-1} - T_i$
30	234.0	1.0	1.0	234.8	1.7	- 0.7	234.7	1.7	0.0
32	237.8	0.3	1.7	238.0	0.6	- 0.2	237.9	0.5	0.1
34	242.9	0.4	1.6	242.9	0.3	0.0	242.6	0.1	0.3
36	248.0	0.6	1.4	247.9	0.5	0.1	247.2	- 0.2	0.7
38	252.9	0.8	1.2	252.8	0.7	0.1	252.1	- 0.1	0.7
40	257.8	0.8	1.2	257.7	0.7	0.1	257.8	0.8	- 0.1
42	263.9	1.3	0.8	263.9	1.3	0.0	263.4	0.8	0.5
44	270.1	2.1	0.0	270.1	2.1	0.0	270.1	2.1	0.0
46	273.7	2.2	- 0.4	274.2	2.8	- 0.5	274.6	3.2	- 0.4
48	274.8	1.6	- 0.6	275.5	2.2	- 0.7	276.0	2.8	- 0.5
50	274.4	1.4	- 0.4	274.7	1.7	- 0.3	275.0	2.0	- 0.3
52	273.0	3.1	0.0	273.0	3.1	0.0	272.9	3.0	0.1
54	270.6	5.7	0.3	270.7	5.9	- 0.1	270.8	5.9	- 0.1
56	266.1	7.3	0.5	266.1	7.3	0.1	265.7	6.9	0.4
58	259.4	8.1	0.8	259.2	7.8	0.2	259.0	7.6	0.2
60	252.0	8.0	1.0	251.6	7.6	0.4	251.2	7.2	0.4
Avg	–	2.8	0.6	–	2.9	- 0.1	–	2.8	0.1

TABLE 14

INVERSION RESULTS FOR EQUATORIAL REGION (JAN 0° N)

Initial Estimate – Jan 10° N

Altitude (km)	1st			2nd			3rd		
	Temp. (°K)	Error		Temp. (°K)	Error		Temp (°K)	Error	
		$T_i - T$	$T_{i-1} - T_i$		$T_i - T$	$T_{i-1} - T_i$		$T_i - T$	$T_{i-1} - T_i$
30	229.4	- 0.6	- 0.4	229.8	- 0.2	- 0.4	230.1	0.1	- 0.3
32	233.1	- 2.0	0.7	233.1	- 2.0	0.0	232.9	- 2.2	0.2
34	237.9	- 2.5	1.3	237.5	- 2.9	0.4	237.1	- 3.2	0.4
36	243.5	- 2.1	1.6	242.7	- 2.9	0.8	241.9	- 3.7	0.8
38	250.6	- 0.3	1.3	249.7	- 1.1	0.9	249.0	- 1.9	0.7
40	257.4	1.4	0.6	256.8	0.8	0.6	256.2	0.2	0.6
42	263.2	1.9	0.0	263.6	2.3	- 0.4	263.6	2.3	0.0
44	268.1	1.9	- 0.7	268.2	2.1	- 0.1	268.2	2.0	0.1
46	271.5	2.2	- 1.2	271.9	2.6	- 0.4	272.1	2.8	- 0.2
48	273.9	3.0	- 1.7	274.6	3.7	- 0.7	275.1	4.2	- 0.5
50	274.1	3.1	- 2.1	275.1	4.1	- 1.0	275.9	4.9	- 0.8
52	271.3	1.1	- 2.2	272.5	2.3	- 1.2	273.4	3.3	- 0.9
54	266.2	- 1.4	- 2.1	267.3	- 0.3	- 1.2	268.2	0.7	- 0.9
56	259.0	- 2.2	- 1.6	259.8	- 1.3	- 0.8	260.6	- 0.6	- 0.8
58	249.4	- 1.2	- 0.8	249.8	- 0.7	- 0.4	250.2	- 0.4	- 0.4
60	240.2	0.2	- 0.2	240.2	0.2	0.0	240.2	0.2	0.0
Avg.	–	0.2	- 0.5	–	0.4	- 0.2	–	0.5	- 0.1

APPENDIX D

PROJECT SCANNER DATA

The following tables (14 through 18) are reproduced from two reports (refs. 12 and 13) issued by NASA, Langley Research Center, describing the results of two sub-orbital launches from the NASA Wallops Station. A summer launch was made on August 16, 1966 followed by a winter launch on December 10, 1966.

Model atmospheres corresponding to atmospheric conditions existing at the time of the experiments were constructed from MRN data obtained within three hours of the flight. Areas within which conditions were reasonably uniform are identified by cell numbers. The longitude and latitude for each cell correspond to the center of the cell. For the winter flight, the model atmosphere for Trout Lake (53° 50'N, 89° 52'W) was assumed to correspond to the winter Cell 1. The reader is cautioned that winter and summer cell numbers do not correspond to the same geographical areas.

The radiance data for all limb scans within a cell were averaged. Although the reports give a considerable number of individual limb scans, only one radiance profile within summer Cells 1, 2, 3, and 7 was used in Section 4 and reproduced in this appendix.

TABLE 15

MODEL ATMOSPHERES DERIVED FROM METEOROLOGICAL DATA FOR THE SUMMER PROJECT SCANNER FLIGHT

Altitude, km	Cell 1 (58° N 68° W)		Cell 2 (53° N 60° W)		Cell 3 (47° N 57° W)		Cell 4 (43° N 45° W)	
	Temperature, °K	Pressure, mb	Temperature, °K	Pressure, mb	Temperature, °K	Pressure, mb	Temperature, °K	Pressure, mb
0	288.0	1010.000	288.0	1010.000	286.0	1012.000	294.0	1025.000
2	277.0	800.511	277.4	800.575	280.1	807.089	284.3	811.321
4	263.2	626.923	264.2	625.462	268.4	634.169	278.2	637.879
6	250.9	477.778	251.3	477.778	257.3	485.542	260.8	489.881
8	234.7	362.245	237.1	364.762	243.3	371.429	246.5	375.253
10	221.7	267.500	221.7	268.487	230.0	277.642	231.3	281.707
12	224.9	196.296	223.8	196.543	217.1	203.652	213.9	207.343
14	224.0	145.370	221.2	145.000	218.0	149.000	213.1	148.810
16	224.0	111.025	222.7	106.884	218.0	110.075	216.5	105.932
18	224.3	79.783	224.0	79.690	219.6	80.161	219.5	81.053
20	225.0	59.065	225.0	59.039	223.1	56.319	222.0	59.115
22	225.6	43.153	225.9	42.702	224.6	43.495	222.6	43.420
24	227.6	31.922	226.0	31.787	225.8	32.132	223.0	31.998
26	232.0	23.590	227.0	23.475	227.2	23.761	225.2	23.583
28	233.6	17.715	228.3	17.491	230.6	17.690	228.1	17.676
30	235.0	13.200	235.0	12.950	237.0	13.170	232.7	13.151
32	237.8	9.910	237.0	9.720	237.0	9.900	238.0	9.740
34	240.6	7.470	240.0	7.320	240.0	7.450	241.0	7.340
36	245.6	5.650	244.0	5.530	245.0	5.640	246.0	5.560
38	252.8	4.310	251.0	4.210	251.0	4.290	250.0	4.240
40	260.0	3.310	258.0	3.230	257.0	3.290	256.0	3.240
42	262.8	2.556	261.0	2.490	260.0	2.535	260.0	2.498
44	256.6	1.971	264.0	1.920	263.0	1.959	263.0	1.930
46	267.0	1.523	265.0	1.491	265.0	1.517	265.0	1.495
48	266.0	1.183	264.0	1.156	265.0	1.177	264.0	1.159
50	265.0	.918	263.0	.895	262.0	.911	262.0	.897
52	261.4	.710	259.0	.691	260.0	.704	261.0	.694
54	258.8	.548	256.0	.532	257.0	.543	260.0	.536
56	257.5	.442	254.7	.431	255.0	.439	257.0	.433
58	256.3	.336	253.3	.331	253.0	.334	254.0	.331
60	255.0	.230	252.0	.230	251.0	.230	251.0	.228
62	246.2	.180	244.4	.180	243.8	.179	243.0	.178
64	237.4	.130	236.8	.130	236.6	.128	235.0	.128
66	229.0	.095	229.0	.095	229.0	.093	227.6	.093
68	221.0	.074	221.0	.074	221.0	.073	220.8	.073
70	213.0	.053	213.0	.053	213.0	.053	214.0	.053

TABLE 15. – Continued

MODEL ATMOSPHERES DERIVED FROM METEOROLOGICAL DATA FOR THE SUMMER PROJECT SCANNER FLIGHT

Altitude, km	Cell 5 (35° N 48° W)		Cell 6 (21° N 55° W)		Cell 7 (17° N 60° W)	
	Temperature, °K	Pressure, mb	Temperature, °K	Pressure, mb	Temperature, °K	Pressure, mb
0	299.0	1023.000	301.0	1016.000	301.0	1016.000
2	284.1	785.377	287.8	808.129	287.8	808.129
4	274.8	639.370	275.2	637.736	275.2	637.736
6	264.5	495.294	259.7	492.669	259.7	492.669
8	250.5	380.612	252.7	379.412	252.7	379.412
10	235.3	287.600	237.1	286.800	237.1	286.800
12	218.2	213.194	220.9	213.014	220.9	213.014
14	204.0	155.000	209.0	154.749	209.0	154.749
16	207.5	112.398	201.0	110.853	201.0	110.853
18	213.0	81.087	205.0	78.659	205.0	78.659
20	217.1	59.074	212.6	57.080	212.6	57.080
22	220.5	43.253	217.5	41.525	217.5	41.525
24	222.7	31.744	219.0	30.412	219.0	30.422
26	225.6	23.350	227.0	22.585	227.0	22.585
28	227.7	17.360	227.7	16.833	227.7	16.839
30	230.0	12.830	227.0	12.390	225.0	12.380
32	239.0	9.620	235.0	9.250	233.0	9.220
34	244.0	7.270	242.0	6.970	241.0	6.930
36	248.0	5.520	247.0	5.290	247.0	5.260
38	251.0	4.220	250.0	4.030	250.0	4.010
40	254.0	3.230	253.0	3.080	253.0	3.070
42	259.0	2.481	259.0	2.370	259.0	2.358
44	264.0	1.917	266.0	1.834	260.0	1.825
46	265.0	1.487	268.0	1.426	270.0	1.420
48	264.0	1.153	265.0	1.108	269.0	1.107
50	262.0	.893	262.0	.859	262.0	.859
52	265.0	.692	267.0	.666	268.0	.667
54	268.0	.538	273.0	.520	273.0	.520
56	264.0	.434	267.0	.422	266.3	.425
58	260.0	.329	261.0	.323	259.7	.330
60	256.0	.225	255.0	.225	253.0	.235
62	248.4	.181	247.8	.181	246.2	.189
64	240.8	.136	240.6	.136	239.4	.143
66	233.4	.102	233.2	.102	232.6	.108
68	226.2	.077	225.6	.077	225.8	.083
70	219.0	.053	218.0	.053	219.0	.058

TABLE 16

AVERAGE OF MEASURED RADIANCE PROFILES FOR 615 cm^{-1} TO 715 cm^{-1} FOR THE SUMMER PROJECT SCANNER FLIGHT

Tangent height, km	Cell 1 (58° N 68° W)		Cell 2 (53° N 60° W)		Cell 3 (47° N 57° W)		Cell 4 (43° N 45° W)		Tangent height, km
	Average radiance, W/m^2-sr	Standard deviation, W/m^2-sr	Average radiance, W/m^2-sr	Standard deviation, W/m^2-sr	Average radiance, W/m^2-sr	Standard deviation, W/m^2-sr	Average radiance, W/m^2-sr	Standard deviation, W/m^2-sr	
10.0	5.91	.08	5.90	.05	5.85	.07	5.73	.17	10.0
11.0	5.93	.08	5.92	.05	5.85	.08	5.75	.15	11.0
12.0	5.95	.07	5.94	.04	5.85	.08	5.77	.14	12.0
13.0	5.95	.06	5.95	.03	5.85	.08	5.79	.12	13.0
14.0	5.97	.04	5.94	.01	5.85	.07	5.80	.11	14.0
15.0	5.97	.03	5.95	.04	5.86	.05	5.80	.11	15.0
16.0	5.98	.03	5.95	.05	5.87	.03	5.79	.11	16.0
17.0	5.98	.04	5.94	.06	5.87	.02	5.77	.11	17.0
18.0	5.97	.04	5.94	.07	5.86	.02	5.74	.10	18.0
19.0	5.95	.03	5.92	.07	5.84	.02	5.71	.10	19.0
20.0	5.92	.03	5.90	.07	5.82	.03	5.66	.09	20.0
21.0	5.88	.03	5.87	.07	5.79	.03	5.62	.09	21.0
22.0	5.84	.04	5.82	.06	5.75	.05	5.57	.09	22.0
23.0	5.78	.05	5.76	.06	5.70	.06	5.50	.09	23.0
24.0	5.71	.07	5.69	.06	5.63	.06	5.43	.08	24.0
25.0	5.62	.08	5.61	.06	5.55	.06	5.34	.08	25.0
26.0	5.51	.08	5.52	.06	5.45	.05	5.24	.08	26.0
27.0	5.39	.08	5.40	.07	5.34	.05	5.13	.07	27.0
28.0	5.26	.08	5.26	.07	5.21	.06	5.00	.08	28.0
29.0	5.11	.09	5.11	.08	5.06	.08	4.86	.09	29.0
30.0	4.96	.09	4.95	.09	4.91	.09	4.71	.10	30.0
31.0	4.81	.09	4.78	.09	4.75	.11	4.54	.11	31.0
32.0	4.63	.09	4.59	.09	4.58	.12	4.36	.11	32.0
33.0	4.45	.10	4.39	.09	4.40	.13	4.18	.11	33.0
34.0	4.24	.10	4.18	.11	4.22	.14	3.98	.11	34.0
35.0	4.02	.11	3.98	.12	4.02	.14	3.77	.11	35.0
36.0	3.80	.12	3.77	.12	3.80	.15	3.55	.12	36.0
37.0	3.57	.13	3.57	.12	3.57	.16	3.32	.12	37.0
38.0	3.36	.12	3.37	.13	3.35	.17	3.09	.13	38.0
39.0	3.15	.10	3.17	.15	3.12	.17	2.88	.13	39.0
40.0	2.92	.07	2.95	.16	2.90	.18	2.68	.13	40.0
41.0	2.70	.07	2.72	.16	2.68	.17	2.49	.14	41.0
42.0	2.48	.07	2.49	.14	2.46	.16	2.30	.15	42.0
43.0	2.28	.06	2.26	.13	2.24	.14	2.11	.15	43.0
44.0	2.09	.06	2.05	.13	2.04	.12	1.91	.14	44.0
45.0	1.90	.06	1.86	.14	1.86	.10	1.72	.12	45.0
46.0	1.73	.06	1.69	.13	1.69	.08	1.54	.11	46.0
47.0	1.56	.07	1.52	.11	1.54	.07	1.38	.11	47.0
48.0	1.41	.08	1.36	.09	1.40	.05	1.23	.11	48.0
49.0	1.25	.08	1.22	.08	1.26	.04	1.09	.10	49.0
50.0	1.10	.08	1.07	.08	1.13	.04	.96	.09	50.0
51.0	.97	.07	.94	.08	1.01	.04	.85	.08	51.0
52.0	.85	.05	.81	.07	.90	.03	.74	.08	52.0
53.0	.74	.04	.71	.07	.80	.04	.65	.07	53.0
54.0	.65	.03	.65	.07	.71	.06	.56	.07	54.0
55.0	.57	.03	.60	.07	.62	.06	.49	.07	55.0
56.0	.52	.03	.53	.04	.54	.07	.43	.07	56.0
57.0	.46	.03	.45	.02	.48	.07	.38	.06	57.0
58.0	.41	.03	.38	.03	.43	.07	.34	.06	58.0
59.0	.34	.03	.31	.04	.38	.07	.30	.05	59.0
60.0	.26	.03	.25	.05	.32	.06	.27	.05	60.0

TABLE 16. – Continued

AVERAGE OF MEASURED RADIANCE PROFILES FOR 615 cm^{-1} TO 715 cm^{-1} FOR THE SUMMER PROJECT SCANNER FLIGHT

Tangent height, km	Cell 5 (35° N 48° W)		Cell 6 (21° N 55° W)		Cell 7 (17° N 60° W)		Tangent height, km
	Average radiance, W/m^2-sr	Standard deviation, W/m^2-sr	Average radiance, W/m^2-sr	Standard deviation, W/m^2-sr	Average radiance, W/m^2-sr	Standard deviation, W/m^2-sr	
10.0	5.49	.14	5.45	.15	5.23	.11	10.0
11.0	5.52	.13	5.46	.14	5.24	.10	11.0
12.0	5.54	.12	5.47	.14	5.25	.09	12.0
13.0	5.55	.11	5.47	.14	5.29	.05	13.0
14.0	5.55	.10	5.48	.13	5.32	.03	14.0
15.0	5.54	.10	5.48	.12	5.34	.03	15.0
16.0	5.53	.10	5.49	.11	5.36	.03	16.0
17.0	5.53	.10	5.49	.10	5.36	.02	17.0
18.0	5.52	.10	5.48	.10	5.36	.02	18.0
19.0	5.51	.11	5.46	.10	5.36	.03	19.0
20.0	5.48	.11	5.44	.11	5.37	.03	20.0
21.0	5.45	.11	5.41	.11	5.37	.02	21.0
22.0	5.40	.11	5.38	.11	5.35	.01	22.0
23.0	5.34	.11	5.33	.11	5.29	.00	23.0
24.0	5.26	.10	5.27	.12	5.23	.01	24.0
25.0	5.19	.10	5.20	.12	5.15	.02	25.0
26.0	5.10	.09	5.11	.12	5.07	.04	26.0
27.0	4.99	.09	5.02	.12	4.99	.05	27.0
28.0	4.88	.09	4.91	.12	4.90	.04	28.0
29.0	4.74	.10	4.78	.11	4.79	.04	29.0
30.0	4.58	.11	4.62	.11	4.66	.04	30.0
31.0	4.41	.13	4.44	.11	4.53	.05	31.0
32.0	4.23	.14	4.26	.12	4.37	.05	32.0
33.0	4.04	.15	4.07	.12	4.19	.06	33.0
34.0	3.83	.15	3.87	.11	3.98	.05	34.0
35.0	3.62	.16	3.66	.12	3.76	.04	35.0
36.0	3.40	.16	3.43	.12	3.55	.04	36.0
37.0	3.19	.16	3.20	.12	3.35	.04	37.0
38.0	2.98	.15	2.98	.12	3.14	.04	38.0
39.0	2.77	.15	2.77	.12	2.91	.05	39.0
40.0	2.56	.15	2.56	.12	2.68	.08	40.0
41.0	2.36	.14	2.36	.12	2.47	.12	41.0
42.0	2.16	.14	2.17	.13	2.29	.15	42.0
43.0	1.97	.13	1.98	.13	2.14	.15	43.0
44.0	1.79	.11	1.79	.14	1.99	.14	44.0
45.0	1.62	.11	1.63	.14	1.84	.13	45.0
46.0	1.45	.10	1.48	.14	1.67	.12	46.0
47.0	1.30	.09	1.33	.14	1.49	.11	47.0
48.0	1.15	.09	1.20	.14	1.32	.10	48.0
49.0	1.02	.09	1.06	.13	1.20	.09	49.0
50.0	.91	.10	.95	.12	1.08	.09	50.0
51.0	.80	.09	.84	.11	.97	.12	51.0
52.0	.70	.09	.75	.12	.86	.13	52.0
53.0	.60	.09	.67	.13	.75	.10	53.0
54.0	.51	.09	.60	.13	.65	.07	54.0
55.0	.44	.09	.52	.12	.55	.07	55.0
56.0	.37	.09	.45	.12	.45	.07	56.0
57.0	.31	.09	.39	.12	.39	.07	57.0
58.0	.26	.09	.34	.12	.33	.07	58.0
59.0	.22	.10	.30	.11	.29	.04	59.0
60.0	.18	.11	.25	.12	.25	.02	60.0

TABLE 17

MEASURED RADIANCE PROFILES FOR 615 cm^{-1} TO 715 cm^{-1} FOR THE SUMMER PROJECT SCANNER FLIGHT

Tangent height, km	Radiance, W/m^2-sr				Tangent height, km
10.0	5.80	5.97	5.84	5.12	10.0
11.0	5.82	5.99	5.84	5.14	11.0
12.0	5.86	5.99	5.83	5.17	12.0
13.0	5.90	5.97	5.82	5.21	13.0
14.0	5.95	5.96	5.82	5.28	14.0
15.0	5.98	5.95	5.83	5.34	15.0
16.0	5.98	5.94	5.84	5.36	16.0
17.0	5.97	5.95	5.85	5.37	17.0
18.0	5.94	5.96	5.84	5.35	18.0
19.0	5.92	5.97	5.82	5.33	19.0
20.0	5.89	5.97	5.81	5.33	20.0
21.0	5.86	5.95	5.79	5.35	21.0
22.0	5.81	5.88	5.77	5.34	22.0
23.0	5.73	5.79	5.74	5.29	23.0
24.0	5.64	5.69	5.68	5.22	24.0
25.0	5.52	5.59	5.60	5.15	25.0
26.0	5.39	5.48	5.51	5.09	26.0
27.0	5.24	5.35	5.40	5.02	27.0
28.0	5.09	5.20	5.28	4.95	28.0
29.0	4.94	5.05	5.16	4.85	29.0
30.0	4.79	4.87	5.02	4.72	30.0
31.0	4.64	4.69	4.88	4.57	31.0
32.0	4.46	4.50	4.73	4.40	32.0
33.0	4.27	4.30	4.56	4.22	33.0
34.0	4.06	4.08	4.36	4.02	34.0
35.0	3.82	3.87	4.15	3.79	35.0
36.0	3.57	3.67	3.93	3.57	36.0
37.0	3.33	3.47	3.72	3.38	37.0
38.0	3.13	3.25	3.50	3.19	38.0
39.0	2.97	3.02	3.26	2.98	39.0
40.0	2.80	2.78	3.03	2.80	40.0
41.0	2.61	2.55	2.81	2.64	41.0
42.0	2.40	2.34	2.60	2.50	42.0
43.0	2.19	2.12	2.39	2.36	43.0
44.0	2.00	1.91	2.18	2.19	44.0
45.0	1.81	1.71	1.98	2.02	45.0
46.0	1.63	1.56	1.79	1.84	46.0
47.0	1.45	1.45	1.62	1.63	47.0
48.0	1.29	1.34	1.46	1.44	48.0
49.0	1.14	1.22	1.31	1.30	49.0
50.0	1.00	1.07	1.17	1.20	50.0
51.0	.89	.92	1.05	1.10	51.0
52.0	.80	.78	.95	1.00	52.0
53.0	.72	.69	.86	.87	53.0
54.0	.65	.63	.78	.75	54.0
55.0	.58	.58	.71	.64	55.0
56.0	.53	.53	.64	.55	56.0
57.0	.47	.45	.58	.49	57.0
58.0	.41	.39	.52	.43	58.0
59.0	.33	.32	.46	.34	59.0
60.0	.26	.25	.39	.26	60.0
LAT.	56.2	52.2	46.3	13.8	LAT.
LONG.	66.5	54.1	48.7	56.3	LONG.
Cell	1	2	3	7	Cell

TABLE 18

MODEL ATMOSPHERES DERIVED FROM METEOROLOGICAL DATA FOR THE WINTER PROJECT SCANNER FLIGHT

Altitude, km	Trout Lake (53°50' N, 89°52' W)	
	Temperature, °K	Pressure, mb
0	246.8	1015.500
2	256.0	792.809
4	249.4	610.593
6	233.3	457.237
8	224.0	339.894
10	218.4	246.918
12	223.7	183.245
14	219.4	134.400
16	217.9	98.158
18	217.0	71.842
20	215.3	52.745
22	215.9	39.317
24	214.7	27.852
26	216.0	20.290
28	216.0	14.816
30	216.0	10.800
32	216.0	7.890
34	219.0	5.780
36	219.0	4.240
38	226.0	3.130
40	226.0	2.320
42	236.0	1.730
44	240.0	1.306
46	244.0	.988
48	251.0	.753
50	251.0	.576
52	251.0	.440
54	250.0	.336
56	250.7	.271
58	251.3	.205
60	252.0	.140
62	248.4	.112
64	244.8	.085
66	241.4	.064
68	238.2	.049
70	235.0	.035

TABLE 19

AVERAGE OF MEASURED RADIANCE PROFILES FOR 615 cm^{-1} TO 715 cm^{-1} (CO_2) FOR GEOGRAPHIC CELL 1 AT 57° N, 92° W FOR THE WINTER PROJECT SCANNER FLIGHT

Tangent height, km	Average radiance, W/m^2-sr	Standard deviation, W/m^2-sr
10.0	4.51	.06
11.0	4.51	.06
12.0	4.50	.07
13.0	4.49	.07
14.0	4.47	.07
15.0	4.46	.06
16.0	4.44	.06
17.0	4.40	.07
18.0	4.34	.08
19.0	4.26	.07
20.0	4.15	.06
21.0	4.08	.05
22.0	4.03	.06
23.0	3.97	.06
24.0	3.90	.06
25.0	3.80	.08
26.0	3.69	.08
27.0	3.57	.07
28.0	3.45	.06
29.0	3.34	.04
30.0	3.19	.03
31.0	3.02	.05
32.0	2.85	.08
33.0	2.69	.11
34.0	2.53	.12
35.0	2.36	.10
36.0	2.20	.09
37.0	2.06	.06
38.0	1.93	.06
39.0	1.82	.07
40.0	1.72	.09
41.0	1.60	.11
42.0	1.46	.12
43.0	1.33	.11
44.0	1.22	.10
45.0	1.15	.08
46.0	1.07	.06
47.0	.97	.05
48.0	.87	.06
49.0	.78	.07
50.0	.70	.05
51.0	.63	.05
52.0	.59	.04
53.0	.57	.02
54.0	.54	.01
55.0	.51	.03
56.0	.47	.05
57.0	.42	.05
58.0	.37	.05
59.0	.36	.04
60.0	.35	.03

REFERENCES

1. Bates, D. R.; and Witherspoon, A. E.: The Photochemistry of Some Minor Constituents of the Earth's Atmosphere (CO_2, CO, CH_4, N_2O). Royal Astronautical Society Monthly Notice, vol. 112, 1952, pp. 101-124.
2. Rodgers, C. D.; and Walshaw, C. D.: The Computation of Infrared Cooling Rate in Planetary Atmospheres. Quart. J. Roy. Meteorol. Soc., vol 92, 1966, pp. 67-165.
3. Kennard, E. H.: Kinetic Theory of Gases. McGraw-Hill Book Co., Inc., 1938.
4. Goody, R. M.: Atmospheric Radiation. Oxford University Press (London), 1964.
5. King, J. I. F.: Theoretical Radiance Profiles for the 15-Micron Carbon Dioxide Band. Proceedings of the Second Symposium on Infrared Sensors for Spacecraft Guidance and Control, Sponsored by USAF Space Systems Division and the Aerospace Corporation, Mar. 14–15, 1967.
6. Elsasser, W. M.: Heat Transfer by Infrared Radiation in the Atmosphere. Harvard University Press (Cambridge), 1942.
7. Elsasser, W. M.: Atmospheric Radiation Tables. Meteorological Monograph, American Meteorological Society (Boston, Mass.) vol. IV, no. 23, August 1960.
8. King, J. I. F.: Modulated Band-Absorption Model. Journal of the Optical Society of America, vol. 55, no. 11 pp. 149–1503, Nov. 1965.
9. Burn, J. W.; Uplinger, W. G.; and Morris, P. P.: Earth Limb Radiance Profiles for the 15-Micron Carbon Dioxide Absorption Band. Lockheed Missiles & Space Company, LMSC-677318, Mar. 10, 1967.
10. Abramowitz, Milton; and Stegun, Irene A., ed.: Handbook of Mathematical Functions. National Bureau of Standards, June 1964.
11. Anon.: United States Standard Atmosphere Supplements. Environmental Science Services Administration, NASA, and USAF, 1966.
12. McKee, T. B.; Whitman, R. I.; and Davis, R. E.: Infrared Horizon Profiles for Summer Conditions for Project Scanner. Langley Research Center, NASA TN D-4741, August 1968.
13. Whitman, R. I.; McKee, T. B.; and Davis, R. E.: Infrared Horizon Profiles for Winter Conditions from Project Scanner. Langley Research Center, NASA TN D-4905, December 1968.

NASA-Langley, 1970 — 20 CR-1513